CHALMERS
UNIVERSITY OF TECHNOLOGY

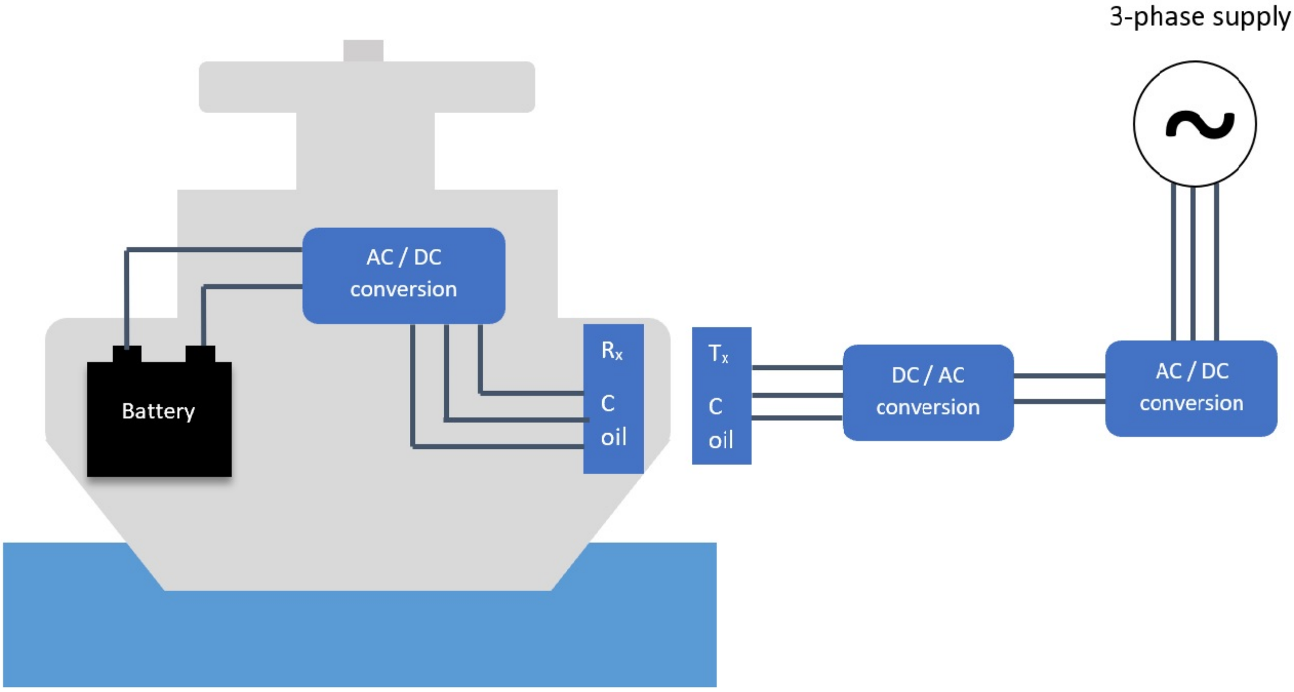

Electric Design of Fast Wireless Charging for Electric Ferries

Master's thesis in Electric Power Engineering

Safoora Qayyum

DEPARTMENT OF ELECTRICAL ENGINEERING

CHALMERS UNIVERSITY OF TECHNOLOGY
Gothenburg, Sweden 2021
www.chalmers.se

Master's thesis 2021

Electric Design of Fast Wireless Charging for Electric Ferries

Safoora Qayyum

CHALMERS
UNIVERSITY OF TECHNOLOGY

Department of Electrical Engineering
Division of Electric Power Engineering
Chalmers University of Technology
Gothenburg, Sweden 2021

Electric Design of Fast Wireless Charging for Electric Ferries
SAFOORA QAYYUM

© SAFOORA QAYYUM, 2021.

Supervisor: Yujing Liu, Chalmers University of Technology
Examiner: Yujing Liu, Chalmers University of Technology

Master's Thesis 2021
Department of Electrical Engineering
Division of Electric Power Engineering
Chalmers University of Technology
SE-412 96 Gothenburg
Telephone +46 31 772 1000

Typeset in LaTeX
Printed by Chalmers Reproservice
Gothenburg, Sweden 2021

Electric Design of Fast Wireless Charging for Electric Ferries
SAFOORA QAYYUM
Department of Electrical Engineering
Chalmers University of Technology

Abstract

Marine transport is an essential part of the transportation system in Sweden. It is transforming conventional energy solutions to sustainable energy solutions to power the vessels. Inductive power transfer (IPT) is an emerging technology for water-borne transport. In this thesis, the use of IPT technology in the marine sector is investigated.

In this thesis, the focus is on a charging system for medium size vessels which run through the Swedish sea and rivers. Three different ferries named Carl Wilhelmson, Tellus, and Adelsöleden are chosen as subject vessels. To implement the fast wireless charging system, the route, schedule, and energy consumption of these vessels are investigated, and the ratings of the energy storage system are proposed based on the available data.

Integration of a fast wireless charging system with the grid is an important part of the whole wireless charging system. Different topologies for single phase and three phase power factor correction (PFC) boost rectifier are studied. Some single phase and three phase PFC boost rectifier topologies are designed and simulated using LT Spice. A comparison between different three phase topologies gives an overview of the best topology to connect the charging system to the grid. The constraints for designing the three phase boost rectifier are V_{out}= 900 V DC and P_{out}= 300 kW. All the designed topologies for three phase gave V_{out} in the range of 850 V DC to 910 V DC and P_{out} 273 kW to 305 kW. The three phase six switch topology is found to be the optimal one with 0.99 input power factor, less than 2% THD, and 98% efficiency.

Keywords: Marine, inductive power transfer, Carl Wilhelmson, charging system, three phase, power factor correction boost rectifier.

Acknowledgements

First, I would like to articulate my deepest gratitude to my supervisor Prof. Yujing Liu for believing in me and providing me support for the completion of the project. I would like to thank Bo Callenberg for sharing his value able knowledge and guiding me throughout my thesis work. It was a good learning experience to work with a marine expert.

I would also like to express gratefulness to Daniel Pehrman and Junfei Tang for their help and cooperation. Sincere thanks to Georgios Mademlis for his value able input and support.

Finally, I would like to take this opportunity to thank my family and friends for their support and encouragement throughout this project.

Safoora Qayyum, Gothenburg, June 2021

Contents

List of Figures

List of Tables

Nomenclature

List of Acronyms

AC	Alternating Current
Ah	Ampere hour
CCM	Continuous Conduction Mode
DC	Direct Current
DCM	Discontinuous Conduction Mode
DoD	Depth of Discharge
ESR	Equivalent Series Resistance
ESS	Energy Storage System
GHG	Greenhouse Gas
IPT	Inductive Power Transfer
kW	Kilo Watt
MOSFET	Metal Oxide Gate Semiconductor Field Effect Transistor
PFC	Power Factor Correction
RMS	Root mean square
SoC	State of Charge
SV PWM	Space Vector Pulse Width Modulation

List of Symbols

CO_2	Carbon Dioxide
D	Duty ratio
I_{ds}	Drain to source current
I_{sc}	Short circuit current
P_{out}	Output power
R_ds	Drain to source resistance
SiC	Silicon carbide
V_{ds}	Drain to source voltage
V_{oc}	Open circuit voltage
V_{out}	Output voltage

1
Introduction

1.1 Background

In modern society, efficient means of transportation play a vital role as a social and economic driver. However, the increasing transportation activities of human beings have put greater pressure on the environment and natural resources. The environment has greatly suffered from greenhouse gases and air pollutants produced by various kinds of vehicles. Moreover, concerns surrounding fossil fuel resource exhaustion have persisted for decades. All the fossil fuels that humans rely on today will eventually run out. Different experts and authorities have given different estimates of how long it will be until the fossil fuels run out. Nevertheless, there is a consensus that if we keep burning the natural resources at the current rate, oil, natural gas, and coal will run out this century [2]. The environmental awareness is raised, people are paying more and more attention to sustainable means of travel, which has driven a lot of innovation of transportation.

Ferries traveling inland rivers and at sea are a competitive alternative to land-based transportation, especially in Sweden. At present, the maritime transport sector is committed to developing green transportation aiming at the reduction of carbon dioxide CO_2 emissions along with other hazardous gases from waterborne transport [3]. There is a rising trend towards the electrification of ferries. Besides, due to the growing popularity of electric vehicles in recent years, charging technologies have been greatly developed, which provides necessary technical supports for ferry electrification.

This thesis work is based on the research on Inductive Power Transfer (IPT) technology under development at Chalmers University of Technology by Yujing Liu and Daniel Pehrman.

1.1.1 Electrification in Marine Sector

The electrification of marine vessels has been evolving for decades to increase functionality, flexibility, and fuel efficiency. The development towards electrification is one of the most promising options currently available towards zero-emission marine transport[4].

Various factors affect the hybridization and electrification of marine vessels, including the commuting route, the number of stops, docking time, onshore and on board battery size, and charging capacity and charging system, etc. In general, short-haul ferries operate on tight schedules with short docking times, meaning that the time available for charging is severely limited. In addition, the amount of energy supplied to the battery at each stop must be sufficient to maintain regular and continuous operation, implying the need for high-power recharging device [5].

1.1.2 Wireless Charging System

Nowadays, most electric or hybrid vessels are charged by plugging a cable into a charging station installed on the harbor. The main drawback of plug-in battery-powered ships is the long charging time compared to the refueling time. The charging time in this type of ship is inevitably includes the time spent on manual or automatic plugging.

A wireless charging system removes the need to plug in and is utilized for easy transfer of power from shore to ship. It replaces the traditional cable method and facilitates a safe connection and disconnection. This method offers a possibility for overcoming the challenges of high-frequency travel and short docking time between ferry crossings for short-haul boats [6]. It reduces maintenance costs as it avoids wear and tear by eliminating the physical connection of electrical components. Furthermore, the use of a wireless charging system also avoids additional difficulties faced by the plug in cable method, due to harsh winter weather conditions and the saline environments.

1.1.2.1 Inductive Power Transfer

Inductive power transfer (IPT) and capacitive power transfer are the two most common wireless power transfer technologies. IPT uses two closely spaced coils. Current flowing in one coil generates a magnetic field, which links to the other coil and induces an emf in it. Electrical energy is transferred from one coil to another through electromagnetic induction. Capacitive power transmission consists of two parallel plates separated by a gap, and the energy transfer to the receiver plate is dependent on the electrical field of both plates.

In this thesis work, the focus is on IPT technology.

A typical IPT system block diagram is shown in Figure 1.1. A direct current (DC) power supply is used to generate a high-frequency sinusoidal current through the inverter, and it creates a high frequency alternating magnetic field on the transmitter side. The electric energy is transferred to the receiver pad from the primary side by magnetic field coupling. The rectifier circuit converts the high-frequency alternating current (AC) voltage into DC voltage on the secondary side of the system. DC voltage is used to charge the battery [7].

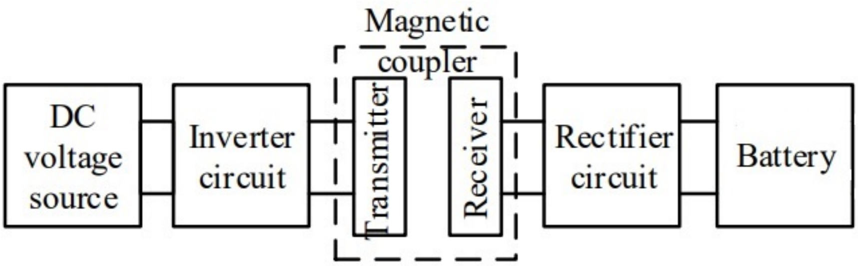

Figure 1.1: IPT system block diagram [7].

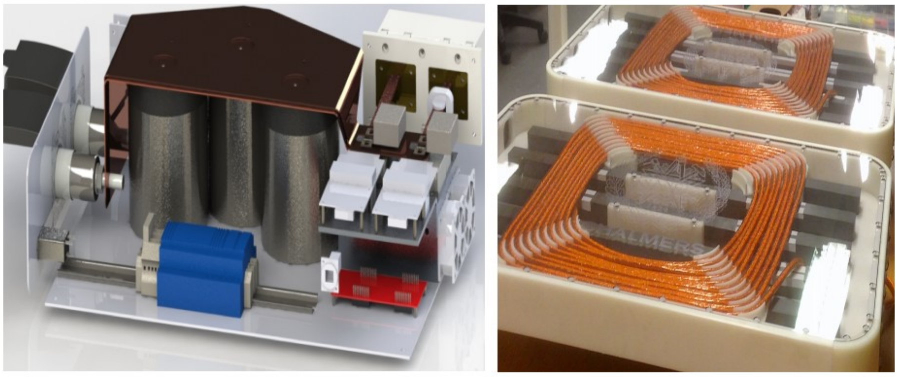

Figure 1.2: 50 kW IPT system developed at Chalmers [**?**].

1.2 Aim of the Project

This thesis aims to design a three phase power factor correction (PFC) boost rectifier to connect with a novel wireless charging system for medium-sized electric ferries used in Swedish rivers and seas. One main task of this thesis is to learn and design the energy storage system for a different type of vessels.

1.3 Scope

The purpose of this thesis is to study electrification in the marine sector. Investigation on the use of IPT technology for medium-size ships and vessels in Sweden. Research on the state of the art of IPT technology for waterborne transportation. Learning about the energy consumption of different diesel-powered passenger ferries and free line ferries running in different parts of Sweden.

Modeling and electrical circuit simulations of the PFC boost rectifier is an essential part of this thesis work. Different topologies of single-phase and three-phase PFC boost rectifier are studied. Some of them are designed and simulated in LT Spice. A comparison between the different topologies is covered in this thesis to find out the most appropriate topology to incorporate with IPT system.

In order to integrate the PFC boost rectifier with the grid a brief study is also done in this thesis. To connect the PFC boost rectifier with on shore supply connection, a transformed is modeled and simulated in LT Spice to verify the proposed fast wireless charging system.

2

Design of On Board Energy Storage System and Vessel Information

In this chapter, the general and technical information about several types of vessels, including passenger and road ferries is presented. A market survey is conducted to collect the data. Their background information is given, the possibility of an IPT system applied to these boats is discussed, and the feasible ratings of the fast wireless charging system are put forward.

2.1 Energy Storage System

To design the energy storage system, the following factors are of importance.

2.1.1 Energy consumption estimation

The estimation of the energy consumption of a vessel is a prerequisite for proposing the ratings of the battery or energy storage system. In this thesis, it is estimated by the following two methods.

- The product of the length of the route or of the time of the trip and the mean energy consumption per unit of length or of time.
  Energy consumed (kWh)= Time of trip (h) x Energy consumed(kWh) / Time(h)

- The product of the fuel consumption for the route and the energy generated per unit of fuel and the efficiency of the engine.

  Energy consumed (kWh)= Fuel consumption (L) x Energy generated(kWh) / Fuel(L) x Efficiency

2.1.2 Battery parameters

Battery ratings are crucial to ascertain that it provides the required energy to the load. Unsuitable ratings of the battery can cause serious problems like permanent battery damage due to over-discharge, low voltage to load and insufficient backup time. The following parameters are of importance in an estimation of a battery.

2.1.2.1 State of charge

The state of charge (SoC) represents the level of the charge available in a battery relative to its capacity. It tells the user how much longer the battery can provide energy. It is measured in percentage (%).

SoC (%)= Charge available / Maximum charge available x 100

2.1.2.2 Charging rate

The charging rate or C rate explains how fast the battery is charged or discharged. Generally, the batteries are rated as 1C. If the battery has a capacity of 2 Ah with 1C, it provides 2 A for one hour. Similarly, if the charging rate is 2C, it provides 4 A for 30 minutes. If the C rate is 0.5C, it provides 1A for 2 hours.

C rate also gives information about the discharge time. 1C means the 1 hour discharge time, 2C means 30 minutes discharge time and, 0.5C means 2 hours discharge time.

2.1.2.3 Depth of discharge

The amount of energy cycled into or out of the battery for a given cycle, expressed as a percentage of battery capacity is known as depth of discharge(DoD). It is the inverse of SoC.

DoD (%)= Charge consumed / Maximum charge available x 100
DoD (%)= 100 % - SoC (%)

2.1.2.4 Battery capacity

The battery capacity is expressed in ampere-hour (Ah) or kWh. It is the current drawn from the battery over a period of time.

Capacity=Electricity x Time duration

As the battery capacity is expressed in kWh so it describes for how long the power can be drawn at the maximum power limit.

Capacity=Power x Time duration

Usually, the fast speed vessels have a limitation on space and weight, so the battery size and volume are important constraints in selection of its capacity.

2.1.2.5 Temperature

Battery capacity and its life are affected by temperature. At a higher temperature, the battery capacity is higher but its life is shortened.

2.1.3 Charging Power

The charging power describes how much energy is needed to charge a battery for uninterrupted operation of an electric ferry.

Charging through IPT technology falls under the category of opportunity charging. In this case, the batteries are charged during the loading and unloading of commuters and vehicles.

There are several factors that are of importance to estimate the charging power for electric ships and vessels.

- Battery charging rate.
- Grid and available network strength at the docking locations.
- Time available for charging.
- Availability of space to install the equipment.

2.2 Investigation of passenger and road ferries

Trafikverket is a Swedish transport organization, which is responsible for rail, road and water transport. Sweden's public transport system mainly consist of Trafikverket's commuter and road ferries. Millions of people move freely around coastal areas as well as in urban and rural districts by using the ferries short-cuts over the water. Public transport through passenger ferries contributes to the development along the rivers and coastal areas.

Ferry routes not only provide an essential public service but also play an important role in goods transportation. These ferries operate with minimal interruption to service and according to their timetable.

Passenger ferries running on long routes, the commuters can board along with the vehicles. The passenger parked the vehicles in a dedicated section of the ferry and seated in a passenger section to enjoy a comfortable journey.

In the case of road ferries during transit, vehicles are collectively transported through road ferries. It is necessary to switch off the engines of the vehicles while being transported from one place to another.

The Swedish state has decided that by 2045 all the means of transport must be climate-neutral. This is a challenge for the passenger vessels as well as for the road ferries [13]. So it is recommended to find fuel alternatives and new smart ways that help to keep a good environment for all.

2.2.1 Carl Wilhelmson

The vessel that is determined as the research target is the passenger ship - Carl Wilhelmson. The owner of the ship is interested in retrofitting it into an electric ferry, in line with current trends in the marine industry.

Carl Wilhelmson is a medium-size ship that could accommodate 180 passengers when it was first built but today can accommodate 220 passengers. The length and the width of the boat are 27.37 m and 6.58 m respectively.

Figure 2.1: Carl Wilhelmson ferry view 1 [9].

Figure 2.2: Carl Wilhelmson ferry view 2 [9].

Carl Wilhelmson was built by Hasse Westers Mekaniska Verkstad AB, Sweden and delivered to Munkedal Trading AB in 1990. In 2011, the boat was sold to Västtrafik AB, Gothenburg and in 2013, the operation and staffing was taken over by Dejlig Cruise AB, Fiskebäckskil.

Since 2012, 2 x Volvo Penta D13 MH, each having crankshaft power of 400 hp (294 kW) propel the vessel. The maximum speed of the vessel is 11 knots.

2.2.1.1 Route and Timetable

The Carl Wilhelmson ferry sails between Lysekil and Skaftö. Figure 2.3 displays the round trip route. The trip over Gullmarsfjorden departs from Lysekil and calls at Östersidan after about 15 minutes, after another 5 minutes, the boat docks in Fiskebäckskil to drive on towards Lysekil again. The total round trip takes about 30 minutes.

Lysekil Harbour is a small port in Sweden. The boat undertakes the transport from Lysekil, and it is also known as the 847 ferry. It starts operation at 6:00 AM and ends at 10:45 PM on weekdays. On Saturdays, its operation hours are 8:30 AM - 10:15 PM and on Sundays 12:10 PM - 9:45 PM. The timetable with the docking

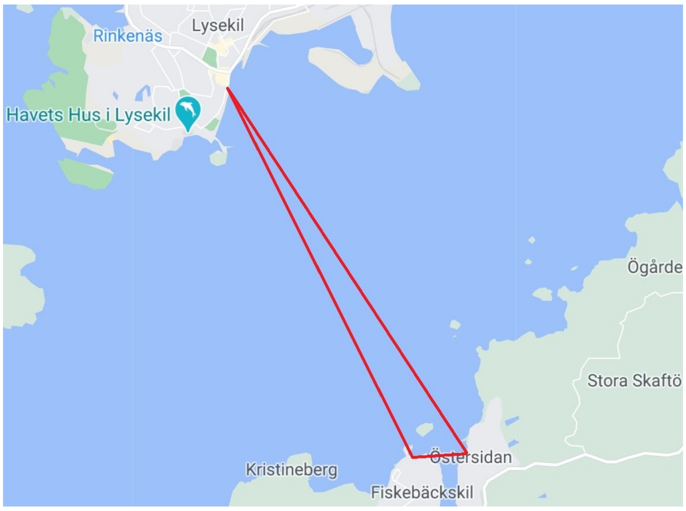

Figure 2.3: The traffic route of Carl Wilhelmson, from Lysekil - Östersidan - Fiskebäckskil and back.

intervals are given below in Table 2.2.

As can be seen, the docking time for the ferry is not consistent, which varies from 0 min (at tour 13, 16, 17, 21 ,and 23) to 55 min (10:20 AM - 11:15 AM). The average interval available for charging after each round trip is 12 min.

2.2.1.2 Specification of Requirements

Table 2.1 presents the diesel consumption and correspondingly the energy consumption of the vessel for a round trip. The diesel consumption of Carl Wilhelmson is 22 liters for one round trip. Generally one liter of diesel generate around 9.5 t0 9.7 kWh of energy. If the diesel engine is assumed to be 30% efficient, the energy consumed by the vessel for a tour is approximately 63 kWh.

Table 2.1: Diesel consumption and kWh of Carl Wilhelmson

Parameters	Values
Diesel	
L/tour	22
kWh/L	9.5
kWh/tour	209
Electricity	
η of diesel engine	0.3
kWh/tour	62.7

Table 2.2 shows the schedule of the Carl Wilhelmson, its energy consumption, state of charge (SoC) of the battery, energy charged by fast wireless charging system during the docking time of the vessel if the IPT system has a power rating of 300 kW .

Table 2.2: Timetable, energy consumption and SoC of 847 ferry (assumption:energy available at the start of day=300 kWh, SoC=100%, rating of propose charging system= 300 kW)

Tour	Depart	Arrival	Docking / Charging time	kWh consumed	kWh available after one tour	SoC (%) after one tour	kWh charged	kWh after charge	SoC(%) after charge
1	06:00	06:30	00:05	63	237	79	25	262	87
2	06:35	07:10	00:05	63	199	66	25	224	74
3	07:15	07:40	00:05	63	161	54	25	186	62
4	07:45	08:15	00:15	63	123	41	75	198	66
5	08:30	09:10	00:05	63	135	45	25	160	53
6	09:15	09:45	00:05	63	97	32	25	122	41
7	09:50	10:20	00:55	63	59	20	275	300	100
8	11:15	11:45	00:05	63	237	79	25	262	87
9	11:50	12:25	00:15	63	199	66	75	274	91
10	12:40	13:10	00:20	63	211	70	100	300	100
11	13:30	14:00	00:05	63	237	79	25	262	87
12	14:05	14:40	00:00	63	199	66	0	199	66
13	14:40	15:15	00:35	63	136	45	175	300	100
14	15:50	16:25	00:15	63	237	79	75	300	100
15	16:40	17:10	00:00	63	237	79	0	237	79
16	17:10	17:40	00:00	63	174	58	0	174	58
17	17:40	18:15	00:40	63	111	37	200	300	100
18	18:55	19:25	00:10	63	237	79	50	287	96
19	19:35	20:10	00:30	63	224	75	150	300	100
20	20:40	21:10	00:00	63	237	79	0	237	79
21	21:10	21:40	00:05	63	174	58	25	199	66.3
22	21:45	22:15	00:00	63	136	45	0	136	45
23	22:15	22:45		63	73	24			

Figure 2.4 shows the SoC of the battery for 300 kW IPT system. At the end of the day, the vessel has more than 20% of charge.

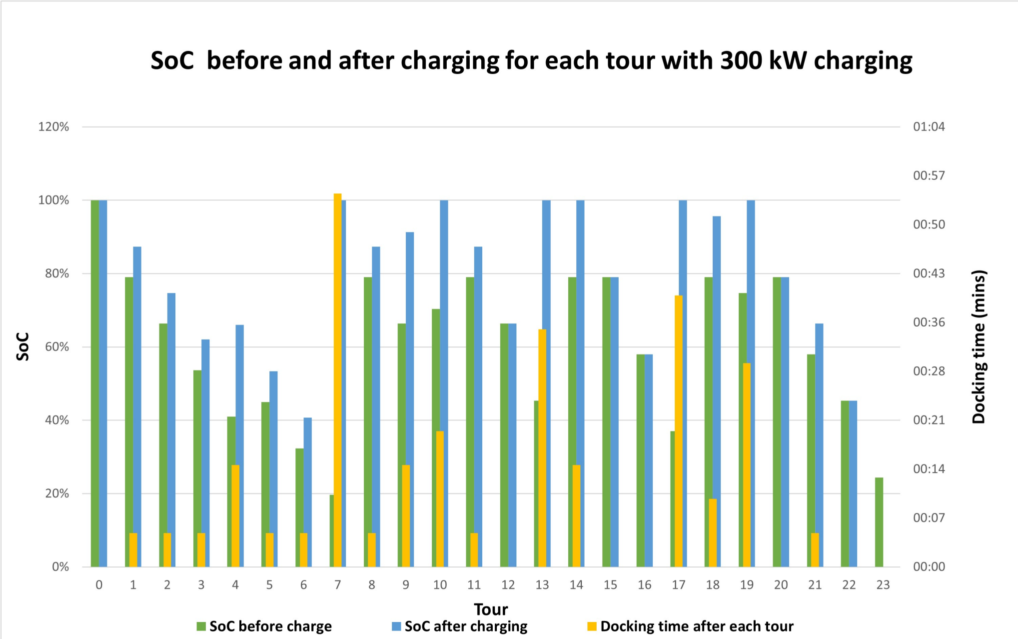

Figure 2.4: SoC and docking time of Carl Wilhelmson with 300 kW charging.

Figure 2.5 shows the comparison of SoC of battery for different power ratings of IPT system. It is clear from the figure that the minimum rating of IPT system should be 300 kW for Carl Wilhelmson to operate it in electric mode.

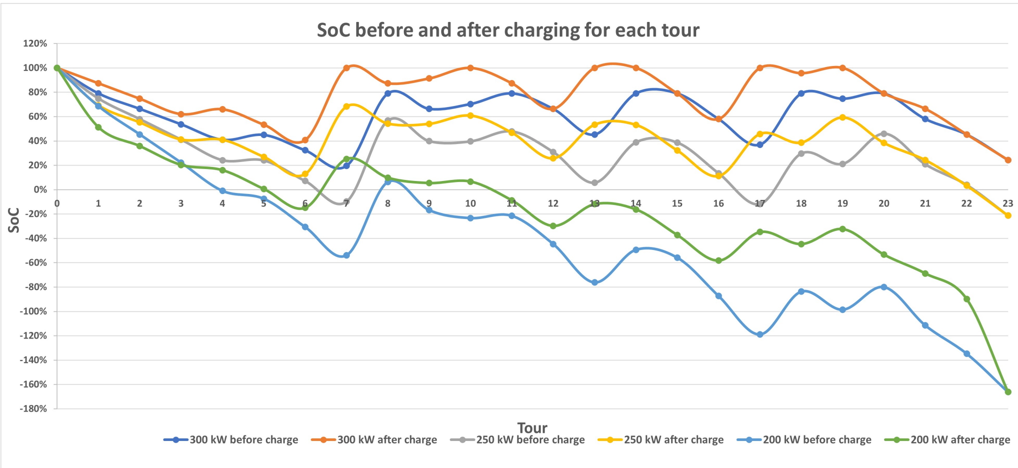

Figure 2.5: Comparison of SoC of battery for different power ratings of IPT system.

With the 300 kW system, the battery SoC goes down to 20% whereas with 250 kW and 200 kW systems the battery is completely drained.

2.2.2 Tellus

This hybrid ferry operates in Sweden on the Gullmarsledan route, a 1.85 km route linking Uddevalla and Lysekil. It is a newly built ferry by shipyard Baltic Workboats AS in Estonia. The dimensions of the ferry are 100m x18m. It has a passenger capacity of 297 and a vehicle capacity of 80 cars. The maximum speed of Tellus is 11 knots.

The ferry operates in a fully electric mode, with batteries charged overnight through an on-shore charging station. On-board diesel engines also charge these batteries while the ferry is in operation. Danfoss Edition delivered the electric power plant and propulsion system of the ferry. The power plant has a capacity of 949 kWh. It is lightweight and is connected to 12 battery racks supplied by Corvus batteries.

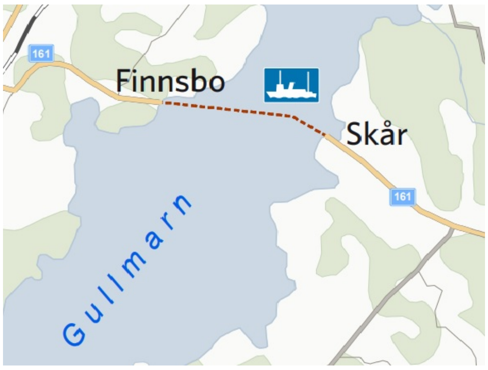

Figure 2.6: Tellus route [11].

Figure 2.7: Tellus[10].

In addition to propulsion control of the ferry, the load control system automatically monitors the power plant. Under non-electric mode, the load control system ensures the optimized fuel consumption. In hybrid electric mode, only one generator set is operated and the battery power is mainly used to propel the ferry.

At present Tellus is already operated in electric mode through batteries, the fast wireless charging can be more easily integrated into Tellus as compared to other road ferries.

2.2.2.1 Specification of Requirements

On the Gullmarsleden route, two ferries named Tellus and Neptunus runs between Finnsbo and skår. The average energy consumption of each ferry is 100 kWh. The energy consumption of the Tellus during a whole day, its docking time, and optimal proposed rating of the fast charging system are summarized in the Table 2.3. The rating of the charging system is proposed by presuming that the onshore charging infrastructure will be built at either Finnsbo or Skår.

As Tellus and Neptunus run on the same route and the onshore charging infrastructure is assumed to be only on one side, the charging time for each free standing road ferry is quite limited. In Table 2.3 the charging power of the IPT system is proposed by considering the already installed battery capacity (950 kWh) of the Tellus.

Table 2.3: Timetable, energy consumption and SoC of Tellus (assumption:energy available at the start of day= 950kWh, SoC=100%, rating of propose charging system= 1400kW)

Tour	Departure	Arrival	Docking/ charging time at Finnsbo	kWh consumed	kWh available after one tour	SoC (%) after one tour	kWh charged	kWh after charge	SoC(%) after charge
1	04:00	04:10	00:00	100	850	89	0	850	89
2	04:20	04:30	00:30	100	750	79	700	950	100
3	05:00	05:10	00:00	100	850	89	0	850	89
4	05:15	05:25	00:05	100	750	79	117	867	91
5	05:30	05:40	00:00	100	767	81	0	767	81
6	06:00	06:10	00:05	100	667	70	117	783	82
7	06:15	06:25	00:00	100	683	72	0	683	72
8	06:30	06:40	00:05	100	583	61	117	700	74
9	06:45	06:55	00:00	100	600	63	0	600	63
10	07:00	07:10	00:05	100	500	53	117	617	65
11	07:15	07:25	00:00	100	517	54	0	517	54
12	07:30	07:40	00:05	100	417	44	117	533	56
13	07:45	07:55	00:00	100	433	46	0	433	46
14	08:00	08:10	00:10	100	333	35	233	567	60
15	08:20	08:30	00:00	100	467	49	0	467	49
16	08:40	08:50	00:10	100	367	39	233	600	63
17	09:00	09:10	00:00	100	500	53	0	500	53
18	09:20	09:30	00:10	100	400	42	233	633	67
19	09:40	09:50	00:00	100	533	56	0	533	56
20	10:00	10:10	00:10	100	433	46	233	667	70
21	10:20	10:30	00:00	100	567	60	0	567	60
22	10:40	10:50	00:10	100	467	49	233	700	74
23	11:00	11:10	00:00	100	600	63	0	600	63
24	11:20	11:30	00:10	100	500	53	233	733	77
25	11:40	11:50	00:00	100	633	67	0	633	67
26	12:00	12:10	00:10	100	533	56	233	767	81
27	12:20	12:30	00:00	100	667	70	0	667	70
28	12:40	12:50	00:10	100	567	60	233	800	84
29	13:00	13:10	00:00	100	700	74	0	700	74
30	13:20	13:30	00:10	100	600	63	233	833	88
31	13:40	13:50	00:00	100	733	77	0	733	77
32	14:00	14:10	00:10	100	633	67	233	867	91
33	14:20	14:30	00:00	100	767	81	0	767	81
34	14:40	14:50	00:10	100	667	70	233	900	95
35	15:00	15:10	00:00	100	800	84	0	800	84
36	15:20	15:30	00:10	100	700	74	233	933	98

Continued on next page

Table 2.3 – continued from previous page

Tour	Depart	Arrival	Docking /Charging time	kWh consumed	kWh available after one tour	SoC (%) after one tour	kWh charged	kWh after charge	SoC(%) after charge
37	15:40	15:50	00:00	100	833	88	0	833	88
38	16:00	16:10	00:05	100	733	77	117	850	89
39	16:15	16:25	00:00	100	750	79	0	750	79
40	16:30	16:40	00:05	100	650	68	117	767	81
41	16:45	16:55	00:00	100	667	70	0	667	70
42	17:00	17:10	00:05	100	567	60	117	683	72
43	17:15	17:25	00:00	100	583	61	0	583	61
44	17:30	17:40	00:05	100	483	51	117	600	63
45	17:45	17:55	00:00	100	500	53	0	500	53
46	18:00	18:10	00:10	100	400	42	233	633	67
47	18:20	18:30	00:00	100	533	56	0	533	56
48	18:40	18:50	00:10	100	433	46	233	667	70
49	19:00	19:10	00:00	100	567	60	0	567	60
50	19:20	19:30	00:10	100	467	49	233	700	74
51	19:40	19:50	00:00	100	600	63	0	600	63
52	20:00	20:10	00:10	100	500	53	233	733	77
53	20:20	20:30	00:00	100	633	67	0	633	67
54	20:40	20:50	00:10	100	533	56	233	767	81
55	21:00	21:10	00:00	100	667	70	0	667	70
56	21:15	21:25	00:05	100	567	60	117	683	72
57	21:30	21:40	00:00	100	583	61	0	583	61
58	21:45	21:55	00:05	100	483	51	117	600	63
59	22:00	22:10	00:00	100	500	53	0	500	53
60	22:20	22:30	00:30	100	400	42	700	950	100
61	23:00	23:10	00:00	100	850	89	0	850	89
62	23:20	23:30	00:30	100	750	79	700	950	100
63	00:00	00:10	00:00	100	850	89	0	850	89
64	00:20	00:30	00:30	100	750	79	700	950	100
65	01:00	01:10	00:00	100	850	89	0	850	89
66	01:20	01:30	00:30	100	750	79	700	950	100
67	02:00	02:10	00:00	100	850	89	0	850	89
68	02:20	02:30		100	750	79			

Figure 2.8 shows the SoC of the battery before and after charging the 950 kWh battery with 1400 kW charging system. The maximum charging time is 30 minutes and the minimum charging time is 0 minutes. With this rating, the minimum SoC of the battery is 35% after completing trip number 14. At the end of the day, the Soc is just below 80%.

A comparison of the SoC of the battery before and after charging the battery for each tour with different power ratings of the charging system is shown in Figure 2.9.

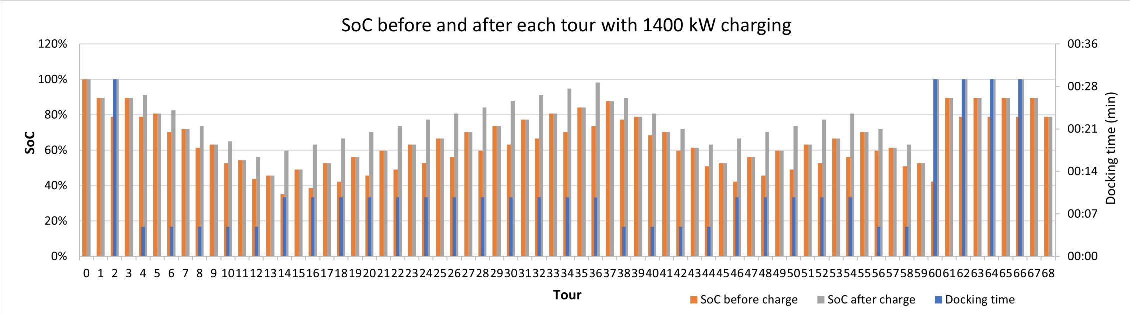

Figure 2.8: SoC and docking time of Tellus with 1400 kW charging.

It is observed that for Tellus the most feasible rating of the IPT charging system is 1400 kW. With a 1300 kW charging rating the SoC goes to almost 3% and with 1350 kW charging power the SoC goes to 20%.

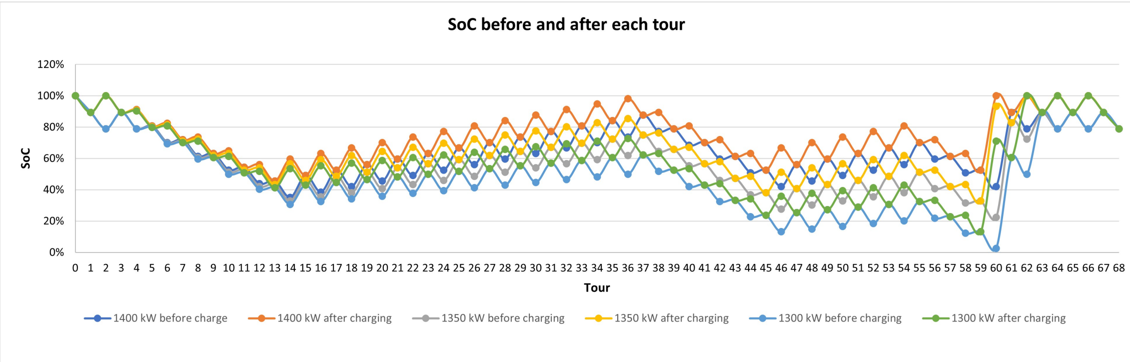

Figure 2.9: Comparison of SoC of battery for different power ratings of IPT system.

2.2.3 Adelsöleden

The Adelsö trail runs in Mälaren islands between Munsö and Adelsö. The ferry route is 1000 meters long and it takes six minutes to go in one direction. The journey between Munsö and Adelsö by road ferry is free of charge.

Figure 2.10: Adelsöleden route [15].

Figure 2.11: Adelsöleden[14].

2.2.3.1 Specification of Requirements

Table 2.4 gives a brief overview of the energy consumption by the Adelsöleden. It completes three round tours in one hour time so the power consumption in one hour is 30 kW.

Table 2.4: Energy consumption by Adelsöleden

Attributes	Values
Distance between Adelsö–Munsö	900 m
Crossing time	6 min
Energy consumption for one side journey	4.5 kWh
Energy consumption during docking time	1 kWh
Total energy consumption for one round tour	10 kWh
kWh/L	9.5
Diesel consumption for one round trip	1.05 L

To install the fast wireless charging technology in Adelsöleden, a study is carried out. The energy consumption of the road ferry can be met with an 80 kW IPT system. Figure 2.12 shows the Soc and the docking time of the Adelsöleden for each round trip with 80 kW fast wireless charging system.

Table 2.5: Timetable, energy consumption and SoC of Adelsöleden (assumption:energy available at the start of day= 80 kWh, SoC=100%, rating of propose charging system= 80 kW)

Tour	Depart	Arrival	Docking / charging time	kWh consumed	kWh available after one tour	SoC (%) after one tour	kWh charged	kWh after charge	SoC(%) after charge
1	05:00	05:19	00:11	10	70	88	14.67	80	100
2	05:30	05:49	00:11	10	70	88	14.76	80	100
3	06:00	06:19	00:01	10	70	88	1.33	71	89
4	06:20	06:39	00:01	10	61	77	1.33	63	78
5	06:40	06:59	00:01	10	53	66	1.33	54	68
6	07:00	07:19	00:01	10	44	55	1.33	45	57
7	07:20	07:39	00:01	10	35	44	1.33	37	46
8	07:40	07:59	00:01	10	27	33	1.33	28	35
9	08:00	08:19	00:11	10	18	23	14.67	33	41
10	08:30	08:49	00:11	10	23	28	14.67	37	47
11	09:00	09:19	00:11	10	27	34	14.67	42	53
12	09:30	09:59	00:11	10	32	40	14.67	47	58
13	10:00	10:19	00:11	10	37	46	14.67	51	64
14	10:30	10:59	00:11	10	41	52	14.67	56	70
15	11:00	11:19	00:11	10	46	58	14.67	61	76
16	11:30	11:59	00:11	10	46	58	14.67	61	76
17	12:00	12:19	00:11	10	51	63	14.67	65	82
18	12:30	12:59	00:11	10	55	69	14.67	70	88
19	13:00	13:19	00:11	10	60	75	14.67	75	93
20	13:30	13:59	00:11	10	65	81	14.67	79	99
21	14:00	14:19	00:11	10	69	87	14.67	80	100
22	14:30	14:59	00:11	10	70	88	14.67	80	100
23	15:00	15:19	00:11	10	70	88	14.67	80	100
24	15:30	15:49	00:01	10	70	88	14.67	80	100
25	16:00	16:19	00:01	10	70	88	1.33	71	89
26	16:20	16:39	00:01	10	61	77	1.33	62	78
27	16:40	16:59	00:01	10	53	66	1.33	54	88
28	17:00	17:19	00:01	10	44	55	1.33	45	57
29	17:20	17:39	00:01	10	35	44	1.33	37	46
30	17:40	17:59	00:01	10	27	33	1.33	28	35
31	18:00	18:19	00:11	10	18	26	14.67	33	41
32	18:30	18:49	00:11	10	23	28	14.67	37	47
33	19:00	19:19	00:11	10	27	34	14.67	42	53
34	19:30	19:49	00:11	10	32	40	14.67	46	58
35	20:00	20:19	00:11	10	37	46	14.67	51	64
36	20:30	20:49	00:11	10	41	52	14.67	56	70
37	21:00	21:19	00:11	10	46	58	14.67	61	76
38	21:30	21:49	00:11	10	50	63	14.67	65	82
39	22:00	22:19	00:11	10	55	69	14.67	70	88
40	22:30	22:49	00:11	10	60	75	14.67	75	93
41	23:00	23:99		10	64	81			

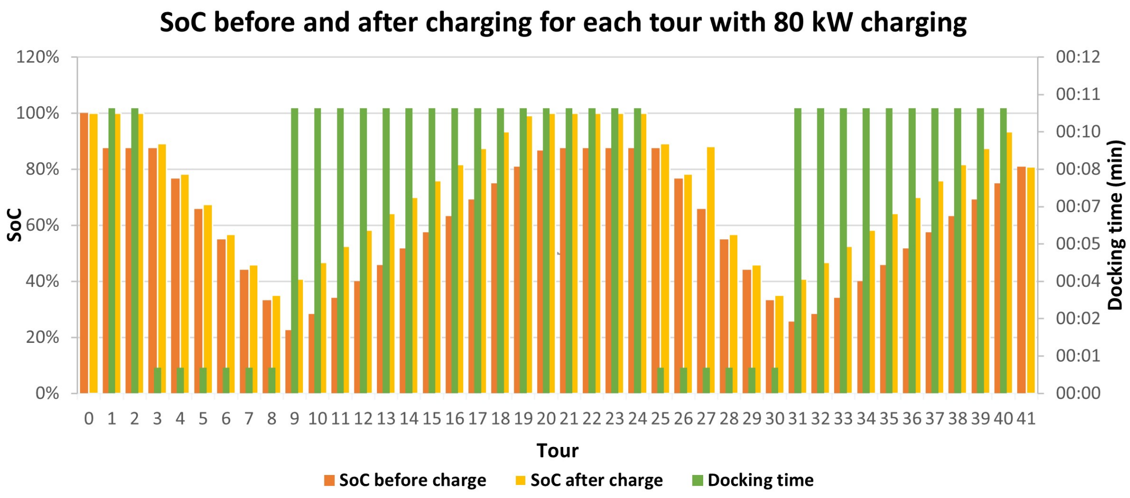

Figure 2.12: SoC and docking time of Adelsöleden with 80 kW charging.

The Figure 2.12 shows that at the end of the day with the proposed 80 kW system, the battery has more than 80% of charge.

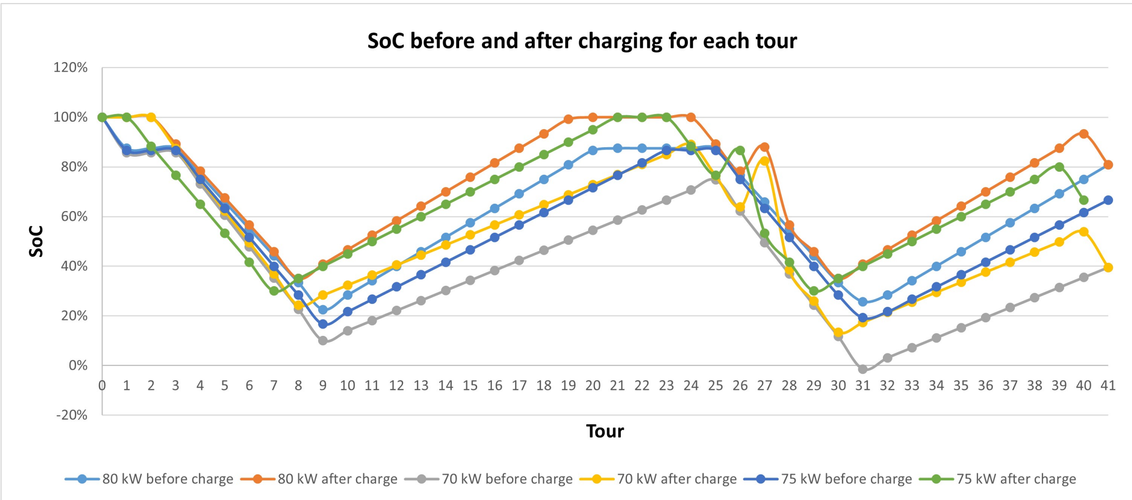

Figure 2.13: Comparison of SoC of battery for different power ratings of IPT system.

A comparison of different ratings of IPT charging system is shown in the Figure 2.13. The most feasible rating for Adelsöleden is 80 kW with which the minimum Soc is 23%. With 75 kW, Soc is reached to 18% and with 70 kW, the 80 kwh battery completely drains out.

Table 2.5 represent the schedule of Adelsöleden. It can be seen that the charging time for the ferry can be 11 minutes which is the same as that of the docking time. But in the case of rush hours from 6 A.M to 7:40 A.M the docking time or charging time is the minimum time for loading and loading the vehicles. Similarly in the afternoon from 3 P.M to 6 P.M the charging time is very small. With 80 kW charging power the battery SoC is more than 80% at the end of the day even with minimum charging time during peak hours.

3

Inductive Power Transfer Technology

This chapter introduces the basic principles of the IPT technology. First, a general concept of IPT technology is discussed. Next, basic principles and compensation topologies are explained using a circuit model. Finally, the state of the art of IPT technology in the marine sector is briefly presented.

3.1 Principle

IPT technology is based on the laws of electromagnetic induction. It uses two induction coils which are separated by a small gap. The primary coil creates an alternating electromagnetic field. The secondary induction coil takes the power from electromagnetic field and convert it back to the electrical energy.

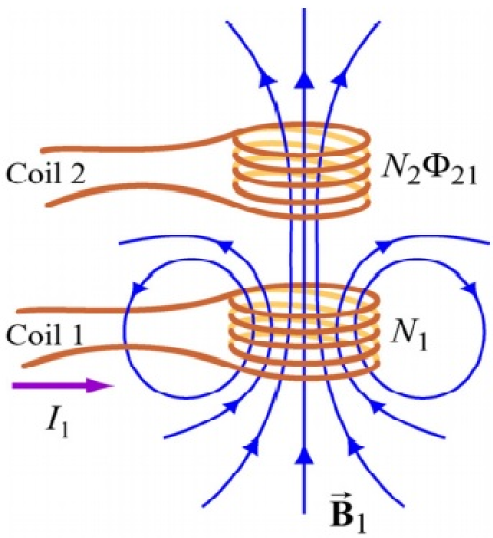

Figure 3.1: The changing current I_1 in coil 1 creates a changing magnetic field B_1 which produces ϕ_{21}[20]

Consider two coils having N_1 and N_2 turns closely spaced to each other. The alternating current I_1 in coil 1 gives rise to magnetic field B_1, proportional to the current

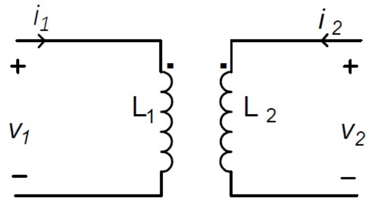

(a) Coupled inductor time domain model.

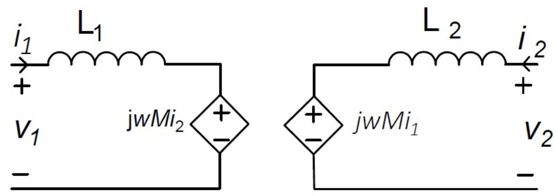

(b) Coupled inductor frequency domain model.

Figure 3.2: Magnetically coupled inductor model.

flowing in the coil. The magnetic flux which is linked to the coil is ϕ_{11}. Since two coils are closely spaced , some magnetic field lines are also passed trough coil 2. So the magnetic flux ϕ_{12} is linked to coil 2. An electromotive force E_{21} is induced in the secondary coil due to this linking flux.

$$E_{21} = N_2 \cdot \frac{d\phi_{21}}{dt} \tag{3.1}$$

The rate of change of magnetic flux coupled with coil 2 is proportional to the rate of change of current in coil 1.

$$N_2 \cdot \frac{d\phi_{21}}{dt} = M \cdot \frac{dI_1}{dt} \tag{3.2}$$

Where M is the proportionality constant known as the mutual inductance. It can be written as

$$M = \frac{N_2 \cdot \phi_{21}}{I_1} \tag{3.3}$$

There are two parameters that plays a crucial role in an optimized inductive transmission.

- High frequency improves the power transfer capability.
- Capacitors, connected the coil creates a resonant system, and increase the power transmission.

3.2 Modeling

Magnetically coupled coils can be model as a traditional transformer. But to transfer power without physical contact, it requires loosely coupled coils. So it has higher leakage inductance as compared to the traditional transformer. The time domain and the corresponding frequency domain model of the coupled inductors are shown in Figure 3.2a and Figure 3.2b.

$$\begin{aligned} v_1(t) &= L_1\frac{di_1}{dt} + M\frac{di_2}{dt} \\ v_2(t) &= L_2\frac{di_2}{dt} + M\frac{di_1}{dt} \end{aligned} \tag{3.4}$$

The corresponding frequency domain equation can be written as

$$
\begin{aligned}
v_1 &= j\omega L_1 i_1 + j\omega M i_2 \\
v_2 &= j\omega L_2 i_2 + j\omega M i_1
\end{aligned} \tag{3.5}
$$

3.3 Maximum Power Transfer for Uncompensated Coils

The performance of magnetically coupled coils is determined by the open circuit voltage V_{oc} of the receiver coil, which is induced by the alternating current in transmitter coil I_1 and the short circuit current of the receiver coil I_{sc} . The maximum VA rating of the coupled coils can be expressed

$$
S_u = V_{oc} \cdot I_{sc}^{*} \tag{3.6}
$$

By (3.5) the V_{oc} and I_{sc} can be expressed by putting $i_2 = 0$ and $v_2 = 0$ respectively.

$$
\begin{aligned}
V_{oc} &= j\omega M i_1 \\
I_{sc} &= \frac{M i_1}{L_2}
\end{aligned} \tag{3.7}
$$

$$
S_u = V_{oc} \cdot I_{sc}^{*} = j\omega \frac{M^2 i_1^2}{L_2} \tag{3.8}
$$

3.4 Compensation topologies

In a contactless inductive power transmission between the primary and the secondary coil, there is an air gap between the coils. Due to this separation, there is a leakage inductance and it reduces the magnetizing flux and mutual inductance. In order to compensate for the leakage inductance and improve the power transmission, a compensation circuit is added to an IPT system. It is achieved by adding capacitors on either side or both sides. It can be added in series or parallel.

There are four main types of compensation topologies:
- SS: Series- series
- SP: Series-parallel
- PS: Parallel- series
- PP: Parallel -parallel

The simplified equivalent circuit of compensation topologies are shown in Figure 3.3.

The basic function of compensation capacitor on the primary side is to minimize the reactive power requirement, hence reducing the VA rating of the power supply. For the secondary side, it minimizes the inductance of the secondary coil, maximizing the power transfer capability.

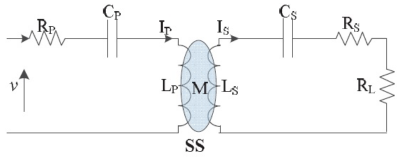

(a) Series-Series compensation[22].

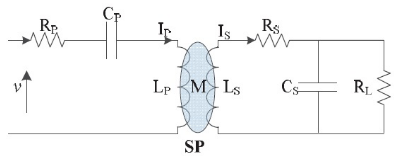

(b) Series-Parallel compensation[22].

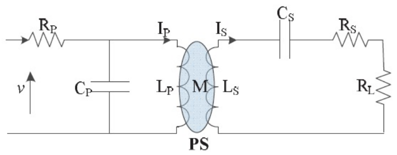

(c) Parallel-Series compensation[22].

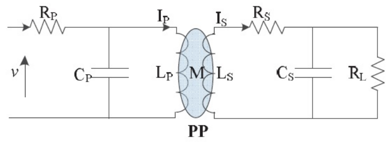

(d) Parallel-Parallel compensation[22].

Figure 3.3: compensation topologies[22].

3.4.1 Series- Series Compensation

The SS choice allows selecting compensation capacitances depending only on the self-inductances, no matter what the load and the magnetic coupling are. Therefore, in case of misalignment between the coil, the system keeps working under resonance dispite of the mutual inductance variations. The equivalent circuit diagram of series series compensation is shown in Figure 3.4 .

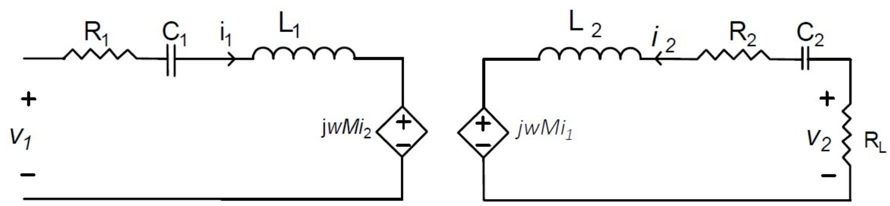

Figure 3.4: Series-series frequency domain equivalent circuit diagram.

For series compensation

$$\begin{aligned} Z_1 &= R_1 + j\omega L_1 + \frac{1}{j\omega C_1} \\ Z_2 &= R_2 + j\omega L_2 + \frac{1}{j\omega C_2} + R_L \end{aligned} \tag{3.9}$$

where C_1 and C_2 are the series compensated capacitors. L_1 and L_2 are showing the self inductance of the coil and R_1 and R_2 are the equivalent series resistance (ESR) of the coils.

3.5 Power Transfer for Compensated Coils

In this project, the series compensation topology has been studied as this topology is practically implemented in an ongoing research at the Chalmers University of Technology.

The maximum power transfer and efficiency expression are derived for the series compensated coils.

$$S_{ss} = V_{oc} \cdot I_{sc}^{*} \tag{3.10}$$

With series- series compensation (3.7) as be written as

$$\begin{gathered} V_{oc} = j\omega M i_1 \\ I_{sc} = \frac{M i_1}{R_s + j\omega L_2 + \frac{1}{jwC_2}} \end{gathered} \tag{3.11}$$

If the coils are completely compensated then

$$I_{sc} = \frac{M i_1}{R_2} \tag{3.12}$$

$$S_{sc} = V_{oc} \cdot I_{sc}^{*} = j\omega \frac{M^2 i_1^2}{R_2} \tag{3.13}$$

3.6 State of the Art

In order to facilitate the reduction in the greenhouse gas(GHG) emissions from the marine sector, International Maritime Organization recommends the development of a charging infrastructures for the electric or hybrid vessels, in particular from renewable energy sources. Several developments in the same direction are emerging globally, and numerous manufacturers and operators in the maritime industry are considering transitioning to clean energy alternatives[23].

Converting or retrofitting diesel-powered ships into hybrid or fully electric results in considerable emission reductions and increased operational efficiency.

With the recent development in IPT technology, some companies and research centers, have proposed their systems to improve the electric mobility through the IPT technology for the shipping industry. Currently, there are two vessels in the Nordic region that operate on the principle of IPT technology. A brief introduction of these vessels is given in the next sections.

3.6.1 Byferga

In Norway, Glomma River divides the city of Fredrikstad into several parts. The city ferries are an important means of Fredrikstad's transport system. Byferga is one of the city ferry, sails between Gamblebyen and Gressvik. It is a newly built electric ferry constructed by Swedeship Marine AB. It is operated by electric propulsion motors with lithium batteries, using wireless induction charging from land.

Figure 3.5: Byferga ferry route[27].

Byferga is 14.95m long, has a passenger capacity of 50, and operates at a maximum speed of 10 knots. It crosses the river six times in an hour, around the clock, seven days a week. The docking time of the ferry is quite limited.

The propulsion system has a main electric engine rated 150 kW. The voltage rating for the main propulsion switch board is 750 V DC with 230 VAC auxiliary voltage and 24 V DC for control and emergency voltage. The backup diesel generator is 60 kW with induction charging of 100 kW from shore. The shore connection is rated with 230 V AC.

Figure 3.6: Byferga ferry [28].

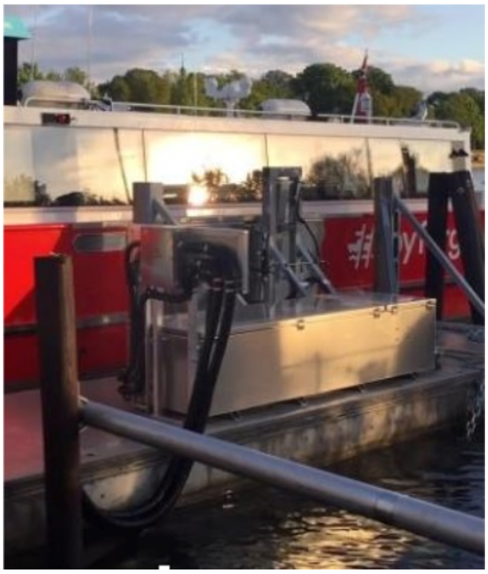

Figure 3.7: Charging of Byferga [31]

The control and integration are taken care of by ZEM-Zero Emission Maritime Solutions. All the cabinets and inverters for microgrid are of Power Tech Sweden which were handed over to ZEM. ZEM provided the 100 kWh energy storage system (ESS) and driveline system. The lithium ion battery installed is 4 X 24 kWh Akasol. The batteries are categorized as propulsion battery, starting battery, consuming battery, and cross connection between battery systems. The propeller has 4-blade, stainless steel duplex. The propulsion inverter is supplied by Danfoss.

The German company IPT Technology developed an inductive charging system for the ferry. The main advantage of the system is the short charging time of the batteries during the limited docking time of the ferry. The inductive charging system consists of two loading plates with coils, one coil with the plate installed on shore and the other coil on the hull of the ship. For loading, the shore side plate is brought close to the ship-side plate. It is charged with an output of around 100 kilowatts. According to IPT Technology, the ship has an average of 112 seconds to charge, each charging is approximately 2 kWh. There are 145 stops during the day that keeps the battery charge level at around 72%. The captain is currently operating the system from the bridge. According to the manufacturer, it should work automatically in the future. It is harmless to passengers and crew and can be used in any weather[31].

3.6.2 M/F Folgefonn

The ferry runs between the islands of Stord, Tysnes, and Huglo in Norway. It has a passenger capacity of 297 and a car capacity of 76. In 2015, the ferry was retrofitted into a full scale plug-in hybrid vessel.

Wärtsilä developed the wireless charging technology based on inductive power transfer. Cavotec and Wärtsilä jointly developed an integrated wireless charging system. As Cavotec provides automated mooring systems for various types of vessels.

Figure 3.8: M/F Folgefonn ferry [29].

Figure 3.9: Inductive Charging System [30].

The system used on the ship is designed to transmit 1 MW of rated power over a range of 15-50 cm between coils. The on board batteries are dimensioned for the transmission system's full charging capacity, but the utilization depends on the chemistry type, the charging interval, and the predicted battery life. With current battery technology, the charging rate is about 2-3 times the nominal battery capacity, but with high power battery chemistry, the charging rate can be up to 6 times the battery capacity.

This solution is best suited for ferries with short docking time and with high power demand. The contact less charging system, which requires minimum maintenance, is an optimal solution for saline environments.

The sources from Wärtsilä show that the vessel can be operated as a hybrid electric and plug-in hybrid. Under the hybrid operation, the savings in fuel consumption in the optimized mode can reach 10–20%. The expected reduction in emission is 30%. Fuel savings are expected to be 20–30% in plug-in hybrid operation and the potential can be 100% in pure plug-in operation.

4

Wireless Charging System

This chapter presents the brief overview of the whole charging system. Each section describes the building block of fast wireless charging system.

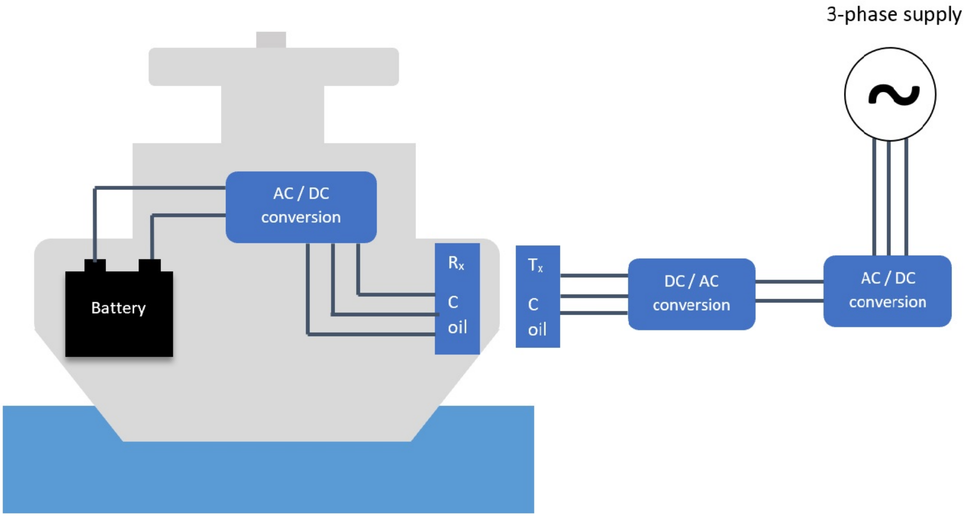

Figure 4.1: Grid to ship system schematic.

4.1 System Description

Figure 4.1 represents the fast wireless charging system from the grid to the vessel. The single line diagram of the system is shown in Figure 4.2. The proposed system is divided into the following parts:

- Substation
- Floating dock/on shore system
- Coil pads
- On board system

Each part of the system consists of different building blocks which are described in the following subsections.

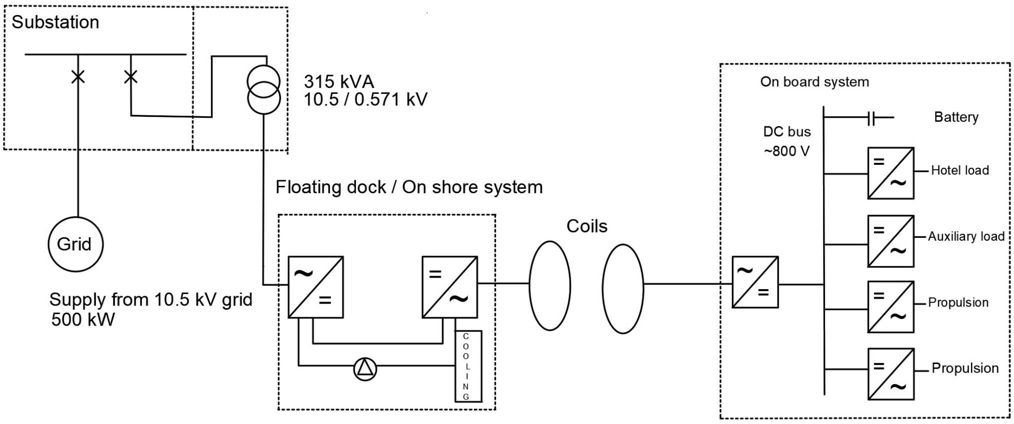

Figure 4.2: Single line diagram of the system.

4.2 Substation

The incoming supply of 10.5 kV, 500 kW is available from the grid. This supply is proposed to connect to the incoming switchgear. The main component of the incoming panel is a circuit breaker. In addition to the circuit breaker, metering and protection equipment is installed in the switch gear.

An out going switch gear is connected to the step down transformer. The outgoing panel is used to protect the incoming supply from any fault from the transformer side.

A step down transformer is used for stepping down the 10.5 kV to 0.571 kV. The incoming panel, outgoing panel, and transformer are placed in a small house called as substation. The outing form the substation is connected to the three phase PFC boost rectifier.

4.2.1 Transformer

The specifications of the selected transformer are presented in Table 4.1.

Table 4.1: Transformer specifications [32]

Parameters	Values
Power kVA	315
Primary voltage kV	10.5
Secondary voltage kV	0.571
Vector group	Dyn11
Cu losses W	3300
e_z %	5.0
e_r %	0.9

The e_z and e_r are the voltage drop across short circuit impedance and short circuit resistance expressed as a percentage of rated voltage.

The transformer with the above specifications is modeled and simulated in LT Spice. Details are presented in Appendix 1.

4.3 Floating Dock/ On Shore System

A floating dock (pontoon) is a structure that floats on water and moves as the water level rises or falls. It is commonly used at harbor. The main purpose of the floating dock is to prevent the water level from changing too much in a year, resulting in too much vertical error between the ship and the fixed dock. With the existence of the floating dock, the deck can be flush with the pontoon vertically when the ship docks, providing a guarantee for passengers to safely and conveniently get on and of the ship.

A part of fast wireless charging system which consists of a PFC boost rectifier and inverter is proposed to install on the floating dock.

This part of the system can also be placed in a housing at the shore.

There can be different feasible solutions for the placement of fast wireless charging but it is not in the scope of this thesis.

4.3.1 Rectifier

The main focus of this thesis work is the design of the power factor control (PFC) boost rectifier. A detailed description of the PFC boost rectifier is presented in Chapter 5.

4.3.2 Inverter

The parameters of the inverter which are required to design the design the PFC boost rectifier are presented in Table 4.2.

Table 4.2: Inverter specifications

Parameters	Values
Input voltage	800 to 900 V DC
Input power	300 kW

4.4 Transmitter and Receiver Coils

The coil pads are an essential part of an IPT system. The transmitter coil is supposed to be installed on the floating dock or on the shore. The receiver coil is usually placed on the ship. The design of coil pads and on-shore and on-board transmitter and receiver coil placement is not in the scope of this thesis.

4.5 On board system

Some part of the IPT system is installed on the vessel. The receiver coil is placed on the vessel. Also, a rectifier which converts the AC voltage to DC voltage is also a part of the on board system. The battery is connected to the rectifier through a DC bus. The propulsion motor, hotel load and auxiliary loads also connected to DC bus.

The ratings of the battery for each of the subject vessel is discussed in Chapter 2.

5

PFC Boost Rectifier

This chapter presents a detailed description of the power factor correction (PFC) boost rectifier.

The purpose of this thesis is to integrate the fast wireless charging system with the grid. Thorough research has been carried out for it. At first, the rectifiers which are available in the market are searched and analyzed. Later, it was decided to design the three-phase power factor correction boost rectifier.

5.1 PFC Boost Rectifier

To feed the DC load from the grid, AC-DC power electronics circuits between the grid and the DC bus are required. If a incoming AC supply is single phase, a single-phase rectifier is used and if the supply is three-phase, a three-phase rectifier is used. AC-DC conversion uses rectifier topologies. The input stage of these AC-DC power converters consists of a bridge rectifier followed by a large filter capacitor.

With the passive AC rectification, the input current is drawn from the grid is non-sinusoidal which results in deteriorated current waveforms. In addition, this process also affects the other users feed from the same grid, causing low power quality with high harmonic current. Also, the utility line cabling, the distribution transformers are affected by these harmonic current values which results in expensive electricity network.
The power factor of the rectifier system can be improved with different methods. These methods are categorized as active power factor correction and passive factor correction. With the active power factor correction method, not only the power factor is improved but also the output voltage can be controlled with the active switches which are used in addition to the diode rectifier. However, in the case of the passive power factor correction method, only passive elements are used to improve the shape of the line current drawn from the grid. Thus, there is no control over the output voltage. The output of the PFC can be boosted using a DC to DC boost converter

In order to establish a connection from the grid (three phase supply) to the on-shore segment of the IPT system, the PFC boost rectifier is an intrinsic part of the whole charging system. The goal of rectification is to provide isolated, regulated DC output, free of input harmonics and with a unity power factor. With the active

PFC rectifier systems, there is a possibility to control the output dc voltage to a constant value, independent of the actual mains voltage and the load.

5.1.1 Single phase PFC Boost Rectifier

Different PFC boost rectifier topologies are shown in Figure 5.1. The conventional boost converter topology uses only one switch, so it is not suitable for high power applications (Figure 5.2a). Interleaved type boost topology (Figure 5.1e) is used to increase the rated power value of conventional boost converters and to reduce the higher switching frequency. However, the use of more controllable switches causes the cost to increase and the control circuit becomes more complex than the conventional type boost circuit.

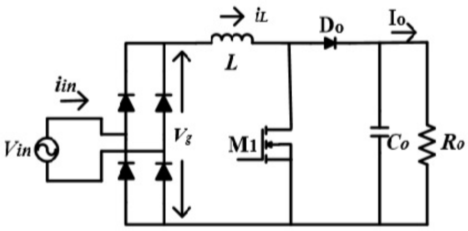

(a) Conventional single phase PFC boost rectifier[33].

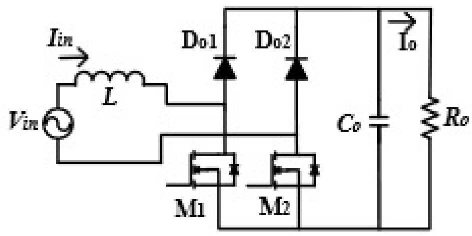

(b) Bridge less boost rectifier[33].

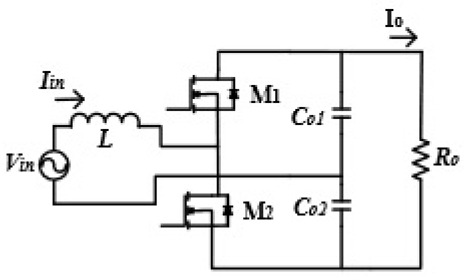

(c) Active half bridge boost rectifier[33].

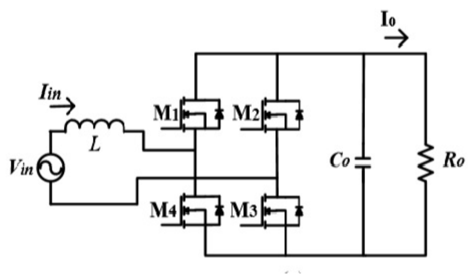

(d) Active full bridge boost rectifier[33].

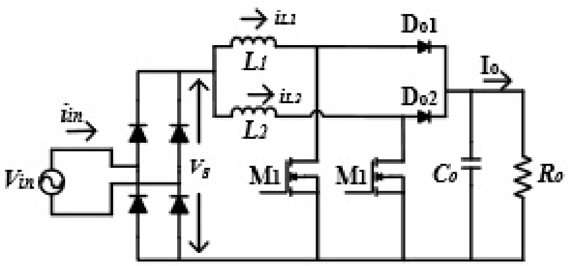

(e) Interleaved boost rectifier[33].

Figure 5.1: Single Phase PFC Boost Converters.

5.1.1.1 Single phase interleaved PFC Boost Converter

Boost converter is the most popular topology for active PFC regulators used in high power applications. In order to reduce the size of the converter and to increase the power density, interleaving technique is utilized.

An interleaved PFC boost converter consist of two boost converters operating in parallel 180° out of phase. The two inductor currents are summed up to give the input current as shown in Figure 5.1e. As the two inductor's ripple current are out of phase they tend to cancel each other and reduce the input ripple current. The best input ripple current cancellation occurs at 50% duty cycle.

The capacitor current is the sum of the two diode currents less than the dc output current. The average output DC current is the sum of the two diode current, as the average current through the capacitor is zero in steady state condition. The diode currents are the function of the duty cycle. As the duty cycle approaches 0%, 50% and 100% the sum of the two diode current approaches dc.

$$\begin{aligned} I_{in} &= I_{L1} + I_{L2} \\ I_{co} &= I_{Do1} + I_{Do2} - I_o \end{aligned} \tag{5.1}$$

5.1.2 Three Phase PFC Boost Rectifier

Different topologies for the three-phase rectifier based on the single-phase PFC boost rectifier are listed below and shown in Figure 5.2.

- Simple boost type converter
- Diode rectifier with PWM regenerative braking rectifier
- Diode rectifier with PWM active filtering
- Vienna Rectifier
- Three phase six switch PFC rectifier

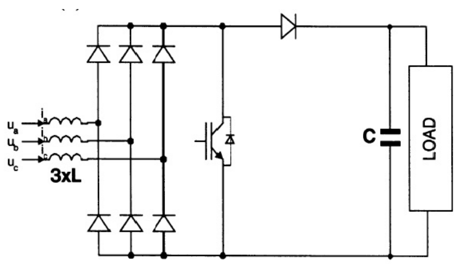

(a) Simple Boost Converter with boost inductor shifted to AC side[37].

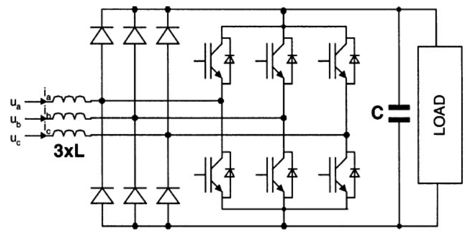

(b) Diode Rectifier with PWM Regenerative Braking Rectifier[37].

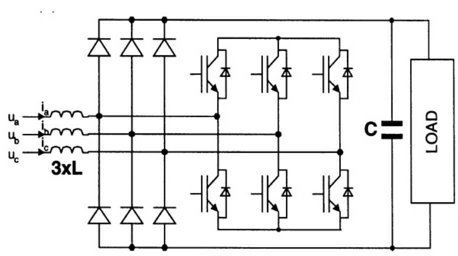

(c) Diode Rectifier with PWM Active Filtering[37].

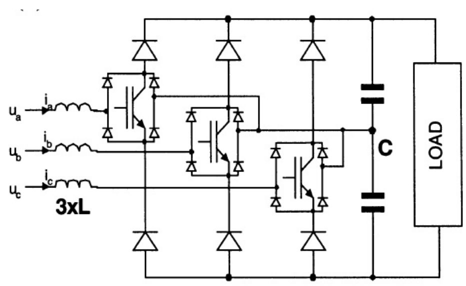

(d) Vienna Rectifier [37].

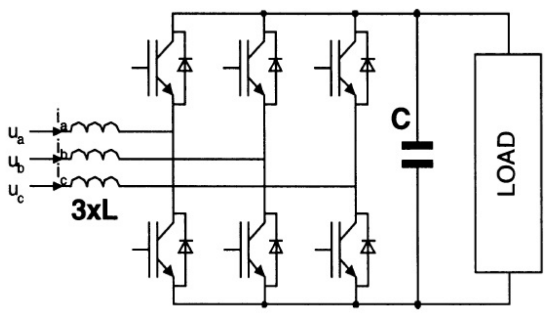

(e) Six Switch Rectifier[37].

Figure 5.2: Three phase PFC Boost Converters.

The comparison of the characteristics of each topology is shown in Table 5.1.

Table 5.1: Comparison of Three Phase Boost Rectifier Topologies

Topology	Regulated DC output Voltage	Low Harmonic Distortion of Line Current	Near Sinusoidal Current waveforms	Power factor Correction	Bidirectional Power Flow
Diode Rectifier	No	No	No	No	No
Boost Type Converter	Yes	No	No	Yes	No
PWM Regenerative Braking Rectifier	No	No	No	No	Yes
PWM Active Filtering Rectifier	No	Yes	Yes	Yes	NO
PWM Vienna Rectifier	Yes	Yes	Yes	Yes	No
PWM Six Switch Rectifier	Yes	Yes	Yes	Yes	Yes

In this thesis, three-phase boost converter with diode converter and six switch PFC rectifier are studied and designed.

5.1.2.1 Three phase Boost Converter with Diode Rectifier

This topology is the three-phase extension of the conventional single-phase boost type diode rectifier. It is hybrid structure having passive three-phase rectifier and then the boost converter with active switch as shown in Figure 5.3.

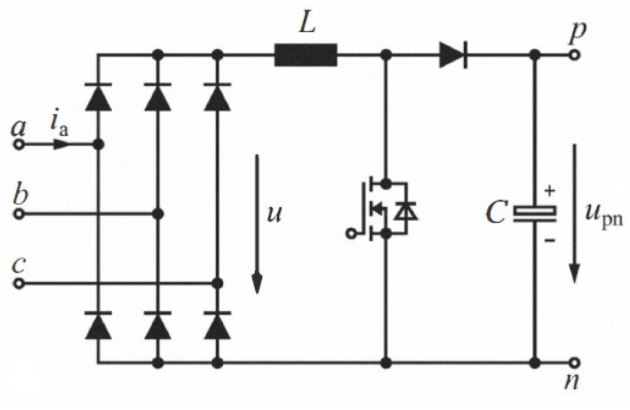

Figure 5.3: Three phase boost converter with diode rectifier[34].

With this topology, the output voltage can be controlled, but the input currents are not of sinusoidal shape, it is of block shape. The current wave shape can be slightly improved if the boost inductances move to the input side.

5.1.2.2 Six Switch PFC Boost Rectifier

In three-phase applications, the six-switch PFC boost rectifier is the most widely used topology because of its good performance and cost effectiveness. It has relatively simple structure as compared to other topologies, despite high functionality.

The overall structure of the three phase boost rectifier is shown in Figure 5.4.

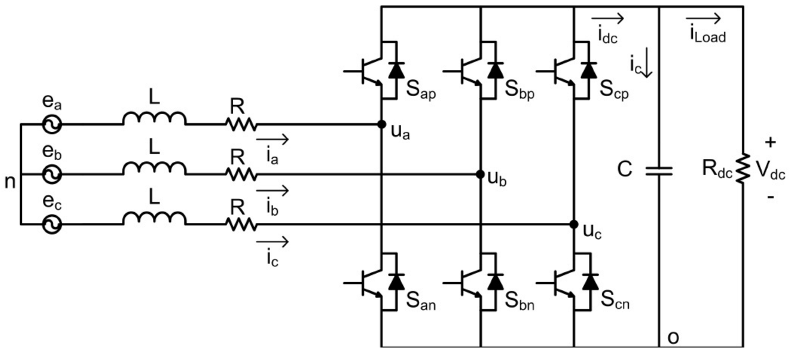

Figure 5.4: Three phase six switch PFC boost rectifier[36].

In this topology, there are three inductances in series with a three-phase ac voltage source. The six MOSFET, two in each bridge leg, are required for voltage regulation and sinusoidal current impression. The inductance reduces the harmonic content by boosting the input ac voltage and filtering the input current.

In general, the operation of a converter can be explained in terms of the input quantities, output quantities and the switching pattern of the MOSFETs. The average output voltage is controlled by controlling the switch on and off duration.

One method for controlling the output voltage is called pulse-width modulation(PWM) switching. This method employs a constant switching time period $T = t_{on} + t_{off}$, hence a constant switching frequency, and adjusting the on duration of the switch to control the average output voltage. In PWM switching, the switch duty ratio D , which is defined as the ratio of the on duration to the total switching time period, is varied.

In other control method, both the switching frequency (hence the time period) and the on duration of the switch are varied. Variation in the switching frequency makes it difficult to filter the ripple components in the input and the output waveform of the converter.

5.1.2.2.1 Operating Principle: The three-phase line voltages and the current are given by the following equations.

$$\begin{aligned} e_a &= E_m Cos(\omega t) \\ e_b &= E_m Cos(\omega t - \frac{2\pi}{3}) \\ e_c &= E_m Cos(\omega t - \frac{4\pi}{3}) \end{aligned} \tag{5.2}$$

$$\begin{aligned} i_a &= I_m Cos(\omega t + \phi) \\ i_b &= I_m Cos(\omega t + \phi - \frac{2\pi}{3}) \\ i_c &= I_m Cos(\omega t + \phi - \frac{4\pi}{3}) \end{aligned} \tag{5.3}$$

As the three phase system is assumed to be balance, the whole circuit can be represented by only one phase. The fundamental frequency components of the three phase supply voltages $u_{a1}(t), u_{b1}(t)$ and $u_{c1}(t)$ and the corresponding fundamental currents $i_{a1}(t), i_{b1}(t)$ and $i_{c1}(t)$ are responsible for the useful power transfer. The basic circuit equation for the fundamental components using Figure 5.4 can be expressed as,

$$e_{a1} = v_{aL1} + u_{an1} \tag{5.4}$$

In phasor form the above equation is

$$\overline{e}_{a1} = \overline{v}_{aL1} + \overline{u}_{an1} \tag{5.5}$$

The fundamental component of the current is given by

$$\overline{i}_{a1} = \frac{\overline{e}_{a1} - \overline{u}_{an1}}{j\omega L} \tag{5.6}$$

Equation 5.6 shows that the magnitude and the angle of line current $\overline{i}_a$ is controlled by the voltage drop across the inductance L interconnecting the three phase ac supply and the converter.

Figure 5.5 shows the corresponding phasor diagram of the (5.5).

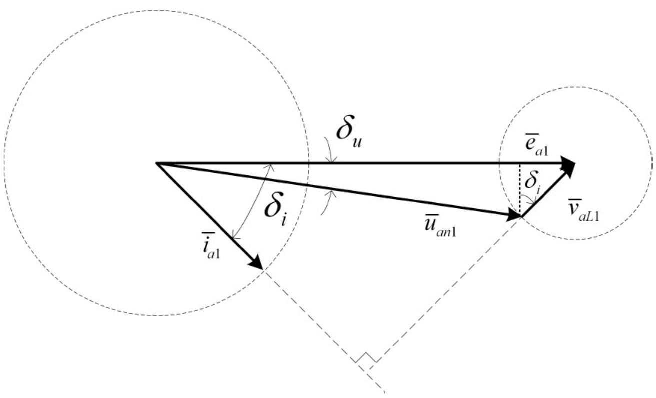

Figure 5.5: Phasor diagram of PFC boost rectifier [36].

The power factor is determined by the angle between $\overline{e}_{a1}$ and $\overline{i}_{a1}$ which is δ_i as shown in Figure 5.5. The line current $\overline{i}_a$ depends on voltage $\overline{u}_{an}$ and the value of inductance L. For a fixed value of supply voltage, the desire value of the current $\overline{i}_a$ can be obtained by varying $\overline{u}_{an}$ and inductance L value.

From Figure 5.5 the following relationships can be obtained.

$$V_{aL1}cos\delta_i = \omega LI_a cos\delta_i = U_{an1}sin\delta_u \tag{5.7}$$

$$V_{aL1}sin\delta_i = \omega LI_a sin\delta_i = E_{a1} - U_{an1}cos\delta_u \tag{5.8}$$

The input active and reactive power can be expressed using (5.7) and (5.8).

$$P_{in} = E_{a1}I_{a1}cos\delta_i = \frac{E_{a1}^2}{\omega L}(\frac{U_{an1}}{E_{a1}}sin\delta_u) = \frac{E_{a1}U_{an1}}{\omega L}sin\delta_u \tag{5.9}$$

$$Q_{in} = E_{a1}I_{a1}sin\delta_i = \frac{E_{a1}^2}{\omega L}(1 - \frac{U_{an1}}{E_{a1}}cos\delta_u) = \frac{(E_{a1}^2 - U_{an1}E_{a1}cos\delta_u)}{\omega L} \tag{5.10}$$

When the power flow from the ac side to the dc side, the converter operates in rectifier mode. In this mode, the $\overline{u}_{an1}$ lags $\overline{e}_{a1}$ by an angle δ_u and the real power is positive. While the $\overline{u}_{an1}$ leads $\overline{e}_{a1}$ by an angle δ_u, the real power is negative and it flow from load (dc side) to the source side(ac side). In this mode the converter is said to be operated in inverter mode.

The values of active power P_{in} and the reactive power Q_{in} depend on $\overline{u}_{an}$ and the value of inductance L. Thus, for a given ac supply voltage and the chosen inductance L value, the active and reactive power can be varied by changing $\overline{u}_{an}$.

In order to achieve a desired value of active output power and the controllable reactive power, the proper switching signals for switches in the three legs of voltage source converter, which decides the required fundamental converter voltage $\overline{u}_{an1}$, are required to generate. The three-phase voltage source converter can provide the regulated DC link voltage and low distorted line side currents with close to the unity power factor operation by varying the amplitude U_{an1} of this fundamental component and its phase shift δ_u with respect to the supply voltage $\overline{e}_{a1}$.

The control strategies for the PWM rectifier are categorized as

- Voltage based control
- Virtual flux based control

The main purpose of the thesis is the use IPT technology for marine application so control is out of the scope of this project. The space vector pulse width modulation (SV PWM) pattern for the MOSFETs is generated by one of my supervisor Junfei Tang. This SV PWM pattern is used for the simulations in LT Spice.

5.2 Rectifier Design and Simulation Results using C3M0016120K

The three-phase and single-phase PFC boost rectifier are designed and simulated in LT Spice. Two topologies are covered in this thesis work. One is the interleaved boost converter and the other is the six switch active boost rectifier.

The details of three-phase rectifier are presented in section 5.2.1 and of single-phase are presented in Appendix B.

5.2.1 Three-phase PFC boost converter with diode rectifier

An interleaved boost converter with diode rectifier for three-phase, is designed and simulated in LT Spice. The schematic for the three-phase system is shown in Figure 5.6.

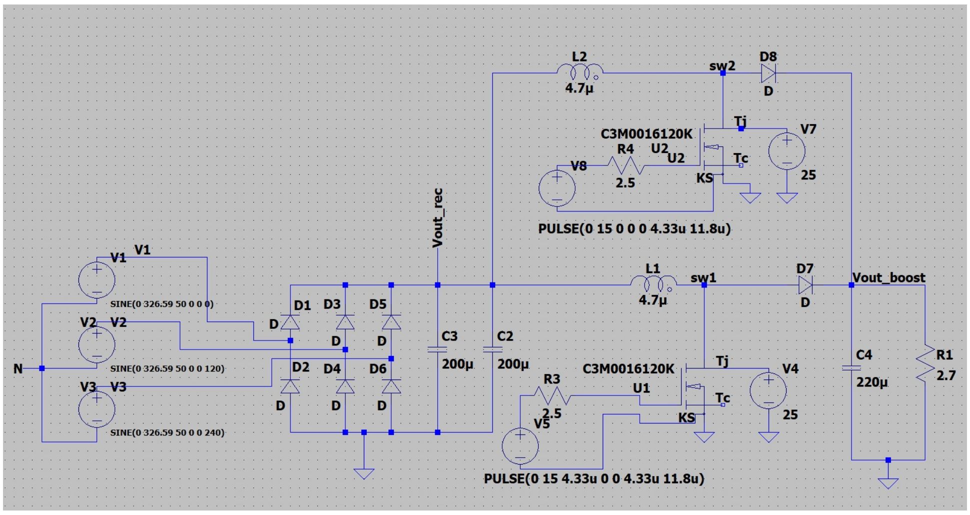

Figure 5.6: Three phase interleaved boost converter.

The input voltage for the three-phase is 400 V line to line rms. For simulation purposes it is converted to maximum phase voltage.

$$
\begin{aligned}
V_{L-Lrms} &= 400V \\
V_{phrms} &= \frac{V_{L-Lrms}}{\sqrt{3}} = 230.94V \\
V_{phmax} &= \sqrt{2} \cdot V_{phrms} = 326.59V
\end{aligned}
\tag{5.11}
$$

The design of the interleaved boost converter involves the selection of inductors, diodes, power switch, input, and output capacitors. It is designed to be operated in continuous conduction mode (CCM) as this is the preferable mode for high power applications [34]. The output power is equally shared by both the legs of the converter so the inductors, diodes, and switches are identical.

In order to get the output power of 300 kW and the DC voltage of 800 to 900 V at the output, C3M0016120K silicon carbide power MOSFET from CREE is selected. It is N channel enhancement mode power transistor. The spice model and library of C3M0016120K from Wolfspeed is imported in LT Spice. The main attributes of the C3M0016120K are stated in Table 5.2.

Table 5.2: C3M0016120k Attributes [38]

Attributes	Value
Channel Type	N
Maximum Continuous Drain Current	115 A
Maximum Drain Source Voltage	1200 V
Maximum Drain Source Resistance	16 mΩ
Maximum Gate Threshold Voltage	3.6 V
Maximum Power Dissipation	556 W
Turn on Delay Time	34 ns
Rise Time	33 ns
Turn off Delay Time	65 ns
fall Time	13 ns

The first step is to calculate the inductor value at the border between the continuous conduction mode (CCM) and discontinuous conduction mode (DCM). It gives an estimation of the inductance value used in converter design. For calculation purposes, the converter is assumed to be lossless.

$$\begin{aligned} V_o &= \frac{V_{in}}{1-D} \\ P_{in} &= P_{out} \\ v_L = L\frac{di}{dt} &= L\frac{\Delta i}{\Delta t} \end{aligned} \tag{5.12}$$

When the MOSFET is conducting the inductor voltage is equal to the input voltage. Thus, the change in the inductor current(ripple current) can be written as

$$\Delta i = \frac{V_{in}D}{Lf_s} \tag{5.13}$$

At the boundary between the CCM and DCM, the average inductor current is half of the ripple current.

$$\begin{aligned} L = \frac{V_{in}D}{2I_Lf_s} &= \frac{V_{in}^2D}{2P_{out}f_s} \\ &= \frac{V_o^2D(1-D)^2}{2P_{out}f_s} \\ L = \frac{V_o^2}{2P_{out}f_s}&(D-2D^2+D^3) \end{aligned} \tag{5.14}$$

To find out the inductance value at the boundary condition, (5.14) is differentiated with respect to the duty cycle. It is found that maximum value of the minimum inductance occurs at D=1/3. By using (5.14)

$$L = \frac{V_o^2 D(1-D)^2}{2P_{out}f_s} \tag{5.15}$$

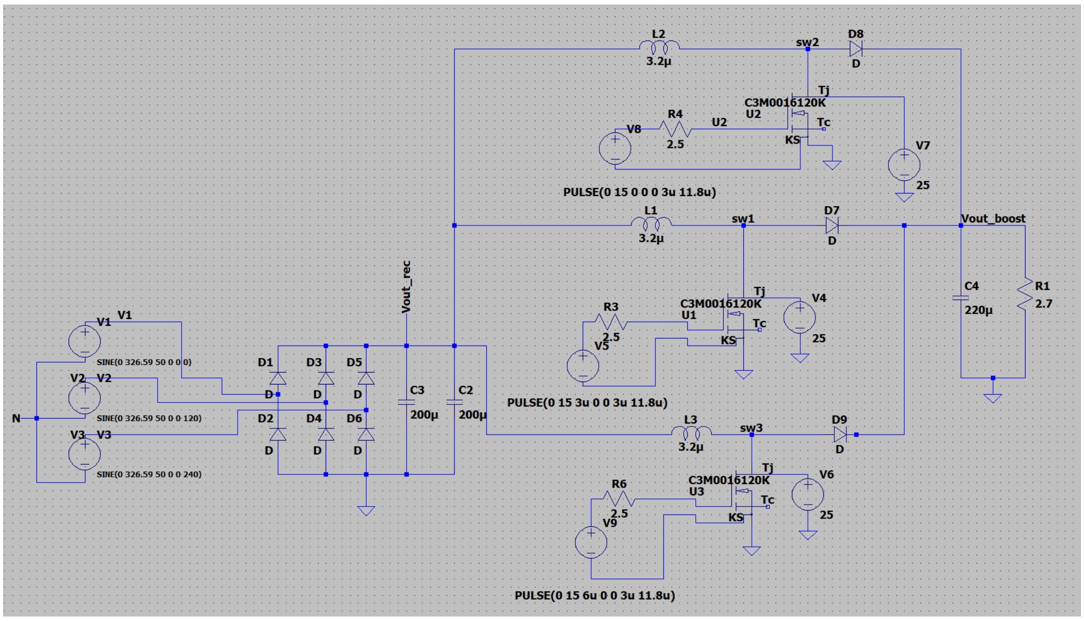

Figure 5.7: Three phase three branches boost converter.

The diodes, inductors and capacitors used for LT Spice simulations are ideal. The MOSFET is modeled in LT Spice by using the actual parameters. The duty cycle is increased to 36.6%. The simulations are run with two switching frequencies 85 kHz and 20 kHz. The inductance value in each branch is 4.7 uH for 85 kHz and 19 uH for 20 kHz to meet the requirements.

The load for boost converter is inverter. It is assumed to be pure resistor for LT Spice simulations. The value of resistor can be estimated from V_{out}=900 V and the P_{out}=300 kW.

$$R_{out} = \frac{V_{out}^2}{P_{out}} = 2.7\Omega \tag{5.16}$$

The required rating of the output power and the output DC voltage is quite high and the switches and diodes are drawing high current, so a three branches PFC boost rectifier has been proposed which is shown in Figure 5.7. In this topology, the switching frequency is the same as that of two branch topology .i.e 85 kHZ and 20 kHZ but the duty cycle is 25.4% as compared to 36.6% in two branch topology. As the current is divided into three branches so the inductance value is also divided into three branches.

5.2.2 Six switch PFC boost converter

The schematic diagram for active three phase six switch rectifier is shown in Figure 5.8.

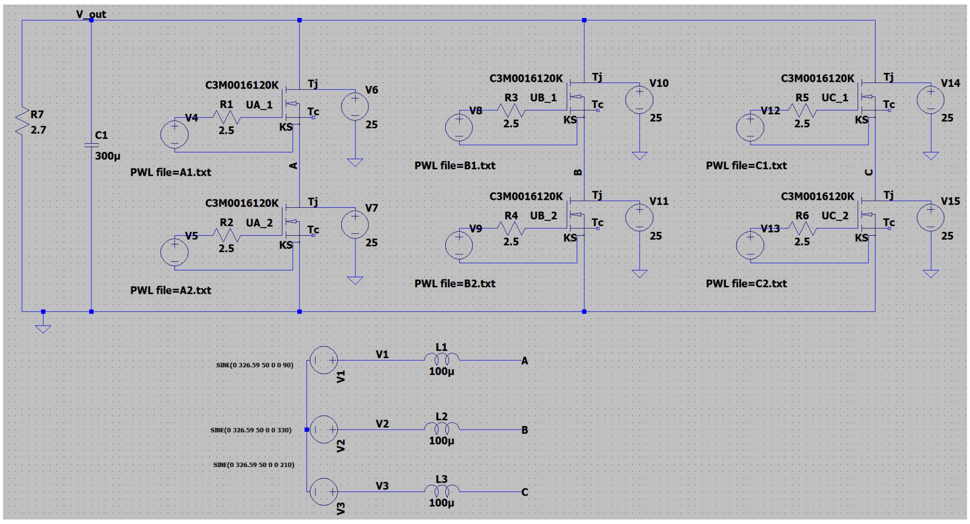

Figure 5.8: Three phase six switch.

The gate to source voltage signal applied to each MOSFET is shown in Figure 5.9.

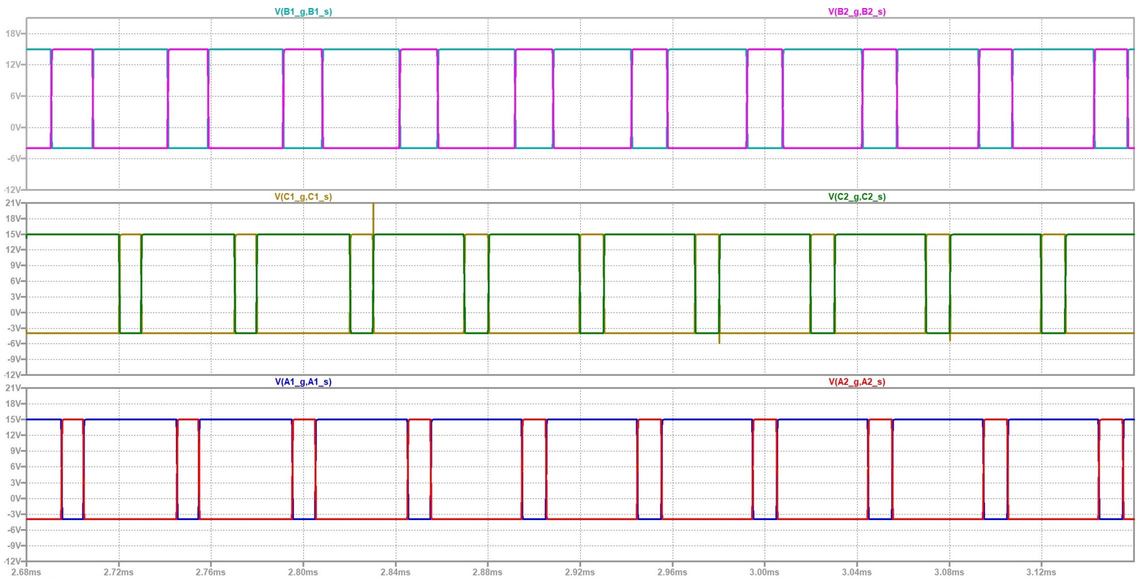

Figure 5.9: Gate signal to the switches.

5.2.3 Simulation Results

The three-phase input voltage for all the topologies is shown in Figure 5.10. The output voltage of the three phase boost converter($V(vout\_boost)$) and the output voltage of bridge rectifier($V(vout\_rec)$) are presented in Figure 5.11. The simulation result of output power of the converter is shown in Figure 5.12.

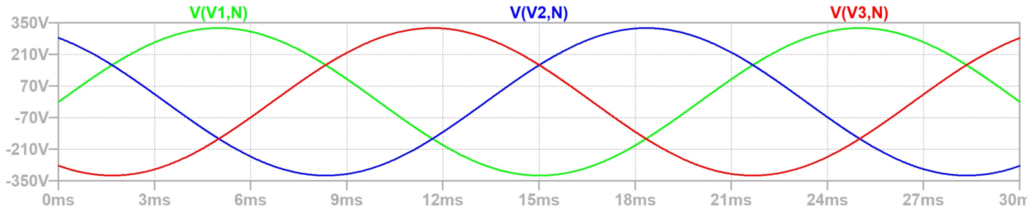

Figure 5.10: Input voltage.

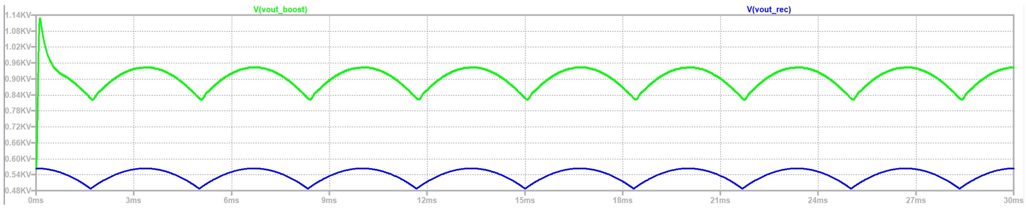

Figure 5.11: Three phase interleaved simulation result: Output voltage.

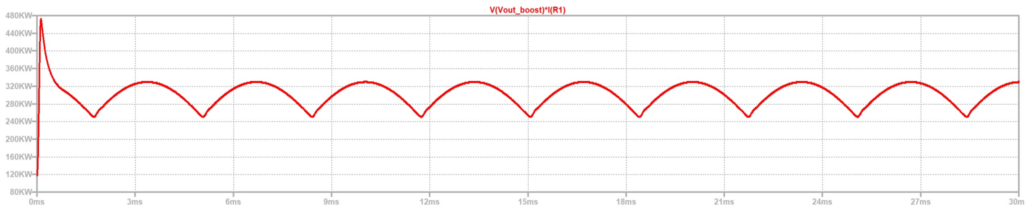

Figure 5.12: Three phase interleaved simulation result: Output power.

The results of three-phase three branches PFC boost rectifier are presented in Figure 5.13 and Figure 5.14.

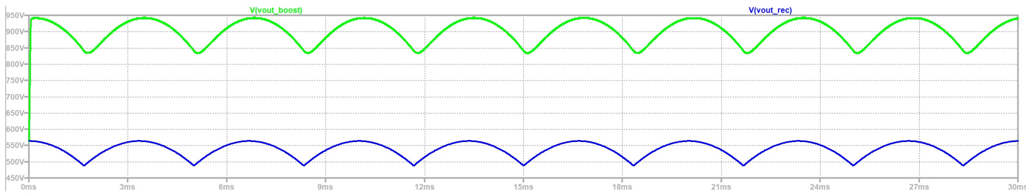

Figure 5.13: Three-phase three branches simulation result: Output voltage.

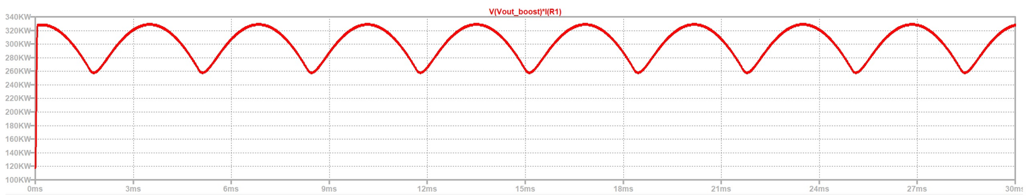

Figure 5.14: Three-phase three branches simulation result: Output power.

The output values which are obtained by simulating the six switch circuit are shown in Figure 5.15 and Figure 5.16.

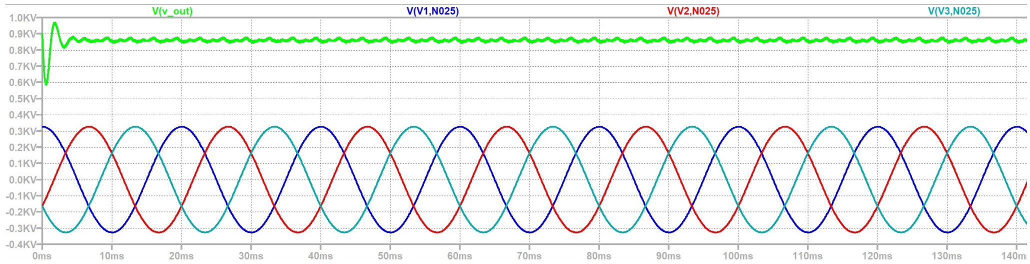

Figure 5.15: Three-phase six switch simulation result: Output voltage.

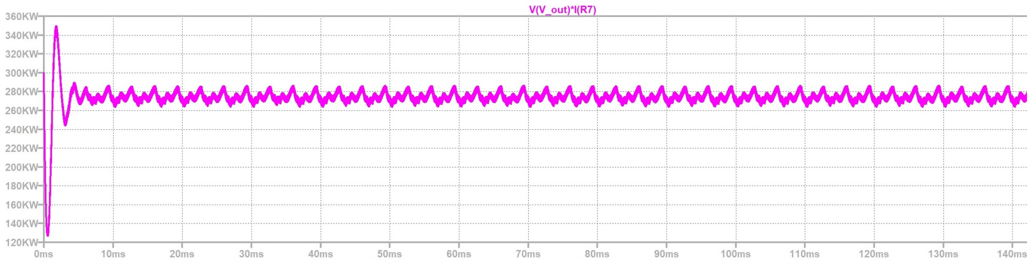

Figure 5.16: Three-phase six switch simulation result: Output power.

The LT spice simulation results are summarized in the Table 5.3.

Table 5.3: Simulation Results

Parameters	Single-phase interleaved		Three-phase 2 branch interleaved		Three-phase 3 branch interleaved		Three-phase six switch
	20 kHz	85 kHz	20 kHz	85 kHz	20 kHz	85 kHz	20 kHz
Output voltage (V)	353	351	907.44	903.05	893.04	901.49	859.82
Output power (kW)	56.373	55.63	305.45	301.6	295.85	301.48	273.96
Input power (kW)	58.40	57.89	317.67	316.07	311.6	317.78	286.88
Power factor	0.98	0.983	0.967	0.966	0.9679	0.9679	0.999
Duty cycle (%)	36.6	36.6	36.6	36.6	25.4	25.4	NA
Drain current (RMS) (A)	92.03	92.9	217	218	172	177	293
Frequency (Hz)	50	50	50	50	50	50	50
THD (%)	3.73	4.59	26.05	26.31	25.88	25.89	1.357
Efficiency (%)	96.51	96.19	96.15	95.45	94.7	94.87	95.49
P_{cond} of MOSFET (W)	135.424	138	753.424	760.38	473.344	501.26	1373.58
P_{sw} of MOSFET (W)	597	679	2606	3039	2526	3499	678.3
P_{loss} of MOSFET(kW)	0.733	0.817	3.36	3.8	3	4	2.055
Total circuit loss (kW)	2.027	2.26	12	14	15.8	16.3	12.92

The current flow through each MOSFET, for each topology is more than its rated current. In order to implement these topologies practically, the switches are put in parallel which in turn reduced the current through each switch. The simulation also are run by putting two or more switches in parallel and different parameters for each topology has been calculated using LT Spice.

In case of parallel switches, the losses of the MOSFET and total losses in the each topology is discussed in section 5.2.5.

5.2.4 Losses in MOSFET

The losses in the MOSFET comprises of switching losses and the conduction losses.

$$P_{loss} = P_{cond} + P_{sw} \tag{5.17}$$

Conduction losses are given by equation

$$P_{cond} = I_{rms}^2 \cdot R_{ds} \tag{5.18}$$

The drain to source resistance R_{ds} of C3M0016120k is 16m Ω and the root mean square (RMS) and average value of the current flowing through the switch for each topology is calculated with LT Spice.

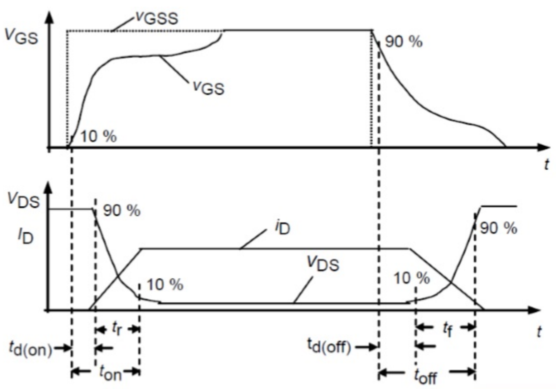

Figure 5.17: Timing waveform of C3M0016120k [38].

Switching losses arises due to the non ideal characteristic of the MOSFET and it also depends on the switching frequency. The switching losses consist of power dissipation during turn on and turn off of the MOSFET.

$$P_{sw} = (W_{sw(on)} + W_{sw(off)}) \cdot f_{sw} \tag{5.19}$$

Refer to the data sheet of the C3M0016120k, $W_{sw(on)}$ and $W_{sw(off)}$ can be approximated as follow.

$$\begin{aligned} W_{sw(on)} &= \frac{V_{ds} I_{ds}}{2} \cdot t_{on} \\ W_{sw(off)} &= \frac{V_{ds} I_{ds}}{2} \cdot t_{off} \end{aligned} \tag{5.20}$$

t_{on} is comprised of turn on delay time and rise time of the MOSFET and t_{off} is the sum of turn off delay time and the fall time.

Table 5.4: Losses in C3M0016120K

Parameters	Single-phase interleaved		Three-phase 2 branch interleaved		Three-phase 3 branch interleaved		Three phase six switch
	20 kHz	85 kHz	20 kHz	85 kHz	20 kHz	85 kHz	20 kHz
I_{drms} (A)	92.03	92.9	222	224	172	177	293
I_{davg} (A)	51	49	124	128	79	83	106
V_{dsrms} (V)	297	297	699	699	645	652	601
V_{dsavg} (V)	206	206	538	538	538	538	425
P_{cond} (W)	135	138	795.66	760.38	473.34	501.264	1373.58
P_{sw} (W)	15.233	62.20	96.78	414.4	60.84	275.18	65.322
P_{loss} (W)	150.233	200.20	893.9	1174.78	534.18	776.44	1438.9

The losses in one MOSFET for each boost rectifier topology are calculated using the analytical expressions are shown in Table 5.4.

Table 5.3 is showing the losses for each MOSFET calculated using LT Spice. The value of switching losses for each topology is larger for LT Spice than the values which are calculated using the analytical expression (Table 5.4).

Analytical calculations are based on some assumptions. The voltage V_{ds} and the current I_{ds} is assumed to have a constant value throughout one cycle and the energy dissipated in turning on and turning off the switch is the same. While in LT Spice simulations, the energy dissipation in turning on and turning off the MOSFET is not the same. Also, the values of V_{ds} and I_{ds} are not constant for one cycle. Thus, there is a difference in the switching loss values calculated with LT Spice and with analytical expressions.

5.2.5 Losses in PFC boost rectifier

The losses in each component of the PFC boost rectifier are calculated with LT Spice. The results are presented in the form of a pie chart and table.

The losses for the parallel combination of switches and the efficiency is shown in Table 5.5.

Table 5.5: Losses in PFC boost rectifier with parallel switches

Losses	Single-phase interleaved (1)		Three-phase 2 branch interleaved(3)		Three-phase 3 branch interleaved(2)		Three phase six switch(4)
	20 kHz	85 kHz	20 kHz	85 kHz	20 kHz	85 kHz	20 kHz
P_{cond} (W)	135.424	138	251.1	253.46	236.672	250.632	343.395
P_{sw} (W)	597	679	2606	3039	2526	3499	678.3
P_{loss} (W)	0.733	0.817	2.857	3.29	2.757	3.749	1.019
Total circuit loss (kW)	2.027	2.26	10.996	12.986	15.087	15.547	6.74
Efficiency (%)	96.53	96.10	96.47	95.75	95.17	95.11	97.65

When two or more switches are put in parallel, R_{ds} is reduced which in turn reduced the conduction losses. The losses are calculated for the different number of parallel switches for each topology and the efficiency of each topology with reduced losses is also calculated. For three-phase two branch interleaved topology, three-parallel switches for each branch are used. For three-phase three branch interleaved topology, two parallel switches for each branch and three phase active six switch topology, four parallel switches for each phase are used.
The results are presented in Figure 5.18, Figure 5.19 and Figure 5.20

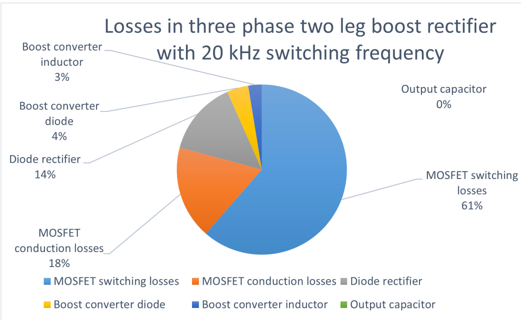

(a) Three phase two leg 20 kHz.

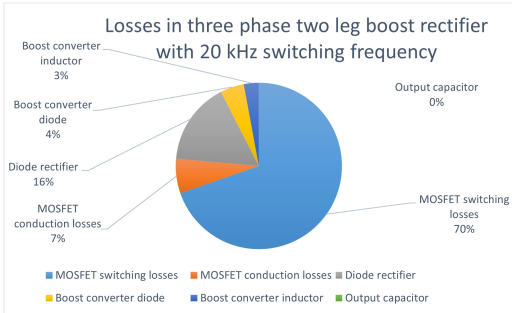

(b) Three phase two leg 20 kHz with parallel switches.

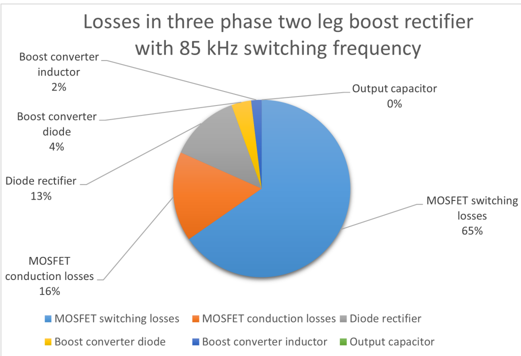

(c) Three phase two leg 85 kHz.

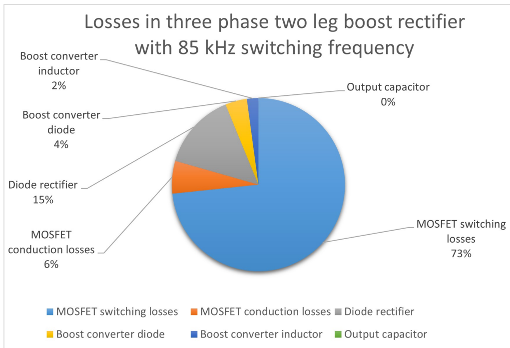

(d) Three phase 85 kHz with parallel switches.

Figure 5.18: Losses in three phase two leg PFC boost rectifier with 20 kHz and 85 kHz switching frequency.

It is clear from Figure 5.18 and Figure 5.19 that with the high switching frequency, the switching losses are increased as shown in Figure 5.18a and Figure 5.18c.

In case of parallel switches, the current through each switch is reduced so the conduction losses of the MOSFET are reduced as shown in Figure 5.19c and in Figure 5.19d.

The losses in the three-phase active six switch topology are shown in Figure 5.20. The conduction losses are reduced due to the parallel switches for each phase.

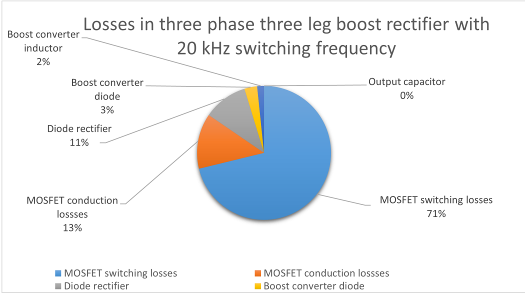

(a) Three phase 3 leg 20 kHz.

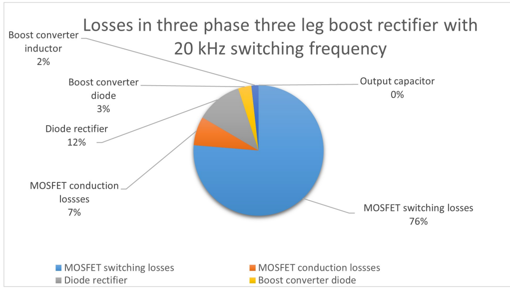

(b) Three phase 3 leg 20 kHz parallel switches.

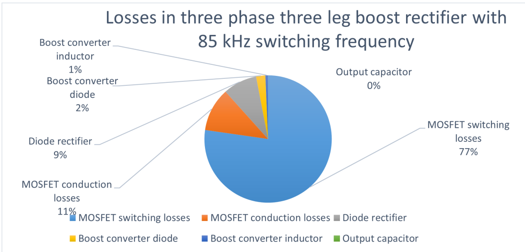

(c) Three phase 3 leg 85 kHz.

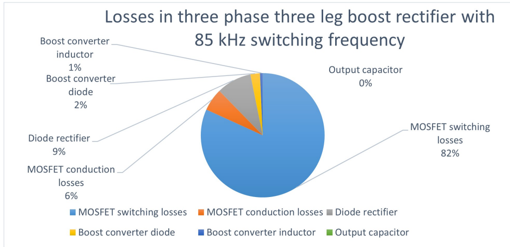

(d) Three phase 3 leg 85 kHz parallel switches.

Figure 5.19: Losses in three phase three leg PFC boost rectifier with 20 kHz and 85 kHz switching frequency.

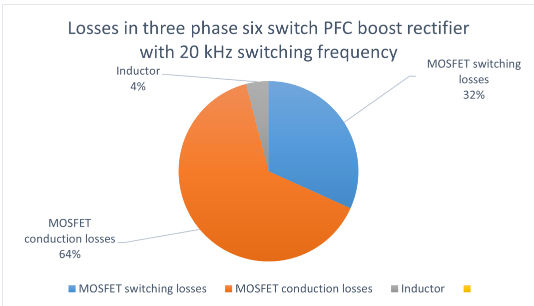

(a) Three phase six switch 20 kHz.

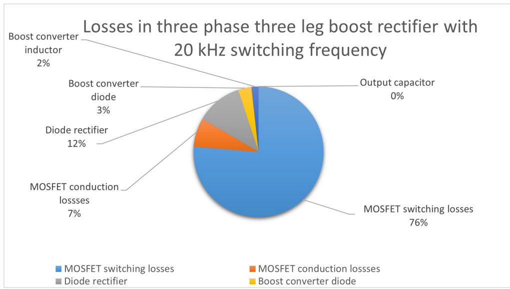

(b) Three phase six switch 20 kHz parallel.

Figure 5.20: Losses in three phase six switch PFC boost rectifier with 20 kHz switching frequency.

5.3 Six switch PFC rectifier with input from the transformer and C3M0016120K

It is proposed that the input side of the rectifier is connected to the three-phase transformer. The secondary side of the transformer is rated as 571 V rms. Details about the transformer can be found in Chapter 4. Table 5.6 shows the results of the simulation with input voltage = 571 V.

The P_{loss} is the sum of switching loss and conduction loss in one switch. The total losses in three-phase PFC are 4.8 kW in which the main contributor is the MOSFET where as the rest of the loss (84 W) occur in inductor.

Table 5.6: Three-phase active PFC rectifier simulation results using C3M0016120K with V_{in}= 571 V

Attributes	Results
Output voltage	880 V
Output power	287 kW
Input power	291.8 kW
Efficiency	98.3%
Drain current (RMS)	211 A
Input power factor	0.99
THD	0.93%
P_{cond}	712 W
P_{sw}	73 W
P_{loss}	786 W
Total losses	4.8 kW

5.4 Three-phase PFC boost Rectifier with CPM3-1200-0013A

To develop the prototype of three-phase active PFC boost rectifier, it is simulated with a MOSFET CPM3-1200-0013A. The reason of selecting this MOSFET from CREE is that there is half bridge module CAB450M12XM3 which has five dies in each switch position. The die is of CPM3-1200-0013A. The three-phase active PFC boost rectifier topology is simulated in LT Spice by scaling down the whole circuit to 5, by using only one MOSFET. In this case the output power requirement is reduced to 1/5 of 300 kW.

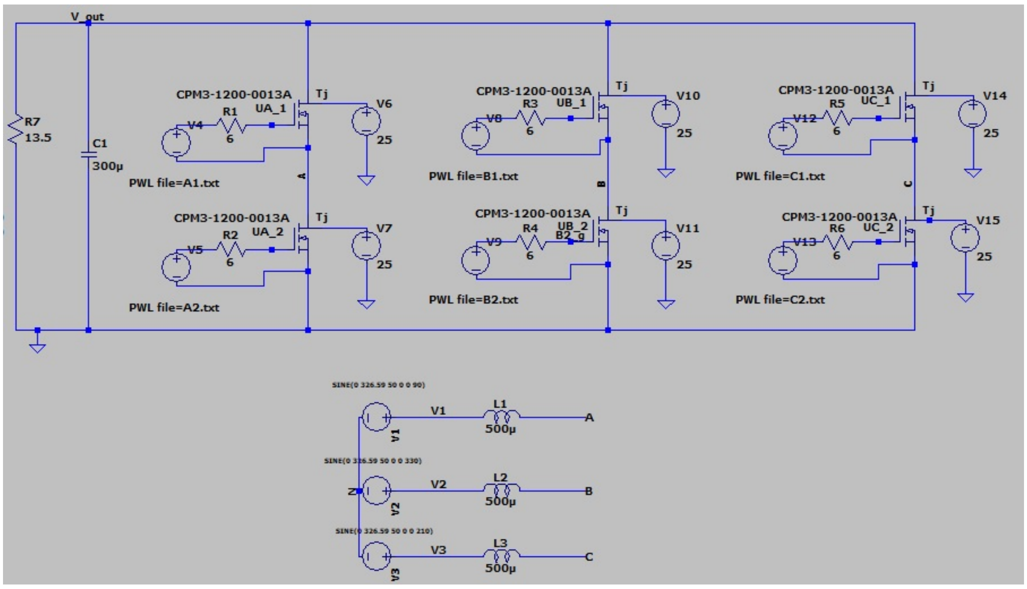

Figure 5.21: Six switch PFC boost rectifier with CPM3-1200-0013A.

The attributes of MOSFET are shown in Table 5.7.

Table 5.7: CPM3-1200-0013A Attributes [39]

Attributes	Value
Channel Type	N
Maximum Continuous Drain Current	149 A
Maximum Drain Source Voltage	1200 V
Maximum Drain Source Resistance	13 mΩ
Maximum Gate Threshold Voltage	3.6 V

5.4.1 Results with $V_{in} = 400V$

The scale down and complete circuit results results are presented in Table 5.8.

Table 5.8: Three-phase active PFC boost rectifier simulation results using CPM3-1200-0013A

Parameters	Scaled down circuit results	Complete circuit results
Output voltage	889 V	889
Output power	58.5 kW	292.5 kW
Input power	59.6 kW	298 kW
Efficiency	98%	98%
Drain current (RMS)	61 A	305 A
Input power factor	0.99	0.99
THD	1.65%	1.65%
P_{cond}	47.44 W	237 W
P_{sw}	137 W	688 W
P_{loss}	185 W	925 W
Total losses	1.1 kW	5.5 kW

The plot of output voltage and output power from LT Spice are presented in Figure 5.22 and Figure 5.23. It can be seen that output voltage has a value of around 900 V DC. The plot of output power showing that the value of output power is around 60 kW.

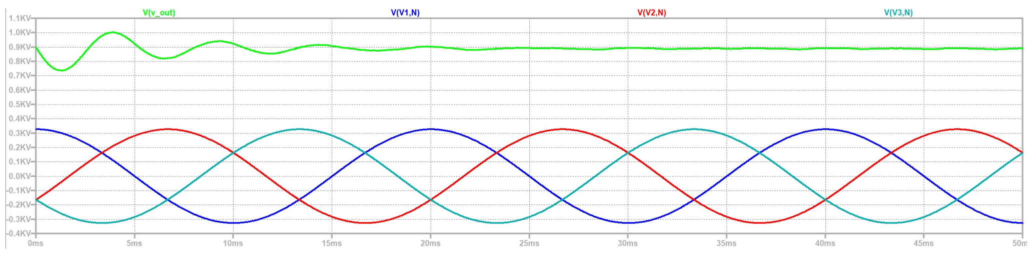

Figure 5.22: DC output voltage and three phase input voltage with CPM3-1200-0013A V_{in}=571V.

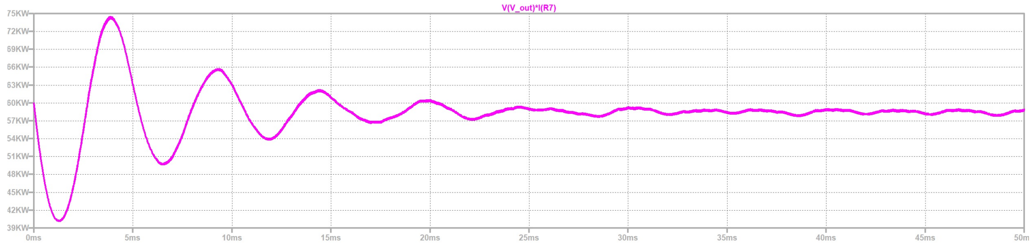

Figure 5.23: Output power with CPM3-1200-0013A V_{in}=571V.

The Figure 5.24 is showing the total losses which occur in the circuit. In this case the switching losses are the dominant one.

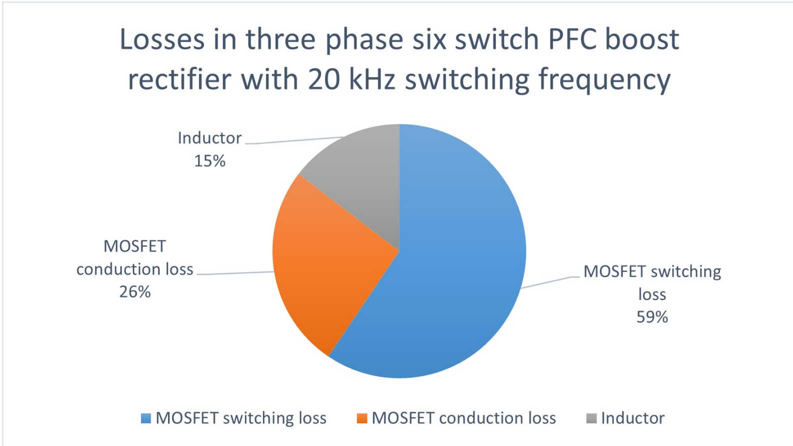

Figure 5.24: Losses in six switch PFC boost rectifier with 20 kHz and V_{in}= 400 V.

5.4.2 Results with $V_{in} = 571V$

The results with v_{in} =571 V are shown in Table 5.9. With the increase in the input voltage, the current through the MOSFETs is decreased. The switching and the conduction losses are also decreased correspondingly.
The plots of output voltage and output power obtained from LT Spice are shown in Figure 5.25 and in Figure 5.26 respectively.

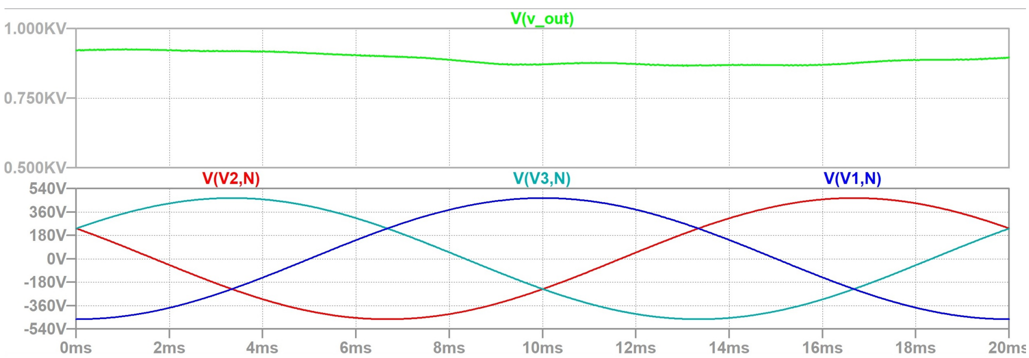

Figure 5.25: DC output voltage and three phase input voltage with CPM3-1200-0013A V_{in}=571V.

Table 5.9: Three-phase active PFC boost rectifier simulation results using CPM3-1200-0013A with V_{in}=571 V

Parameters	Scaled down circuit results	Complete circuit results
Output voltage	891 V	891 V
Output power	58.8 kW	294 kW
Input power	59.2 kW	296 kW
Efficiency	99%	99%
Drain current (RMS)	43 A	215 A
Input power factor	0.99	0.99
THD	0.23%	0.23%
P_{cond}	22.18 W	111 W
P_{sw}	53 W	265W
P_{loss}	75.6 W	378 W
Total losses	0.453 kW	2.26 kW

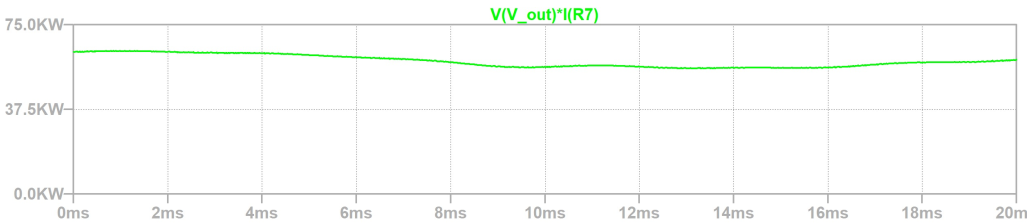

Figure 5.26: Output power with CPM3-1200-0013A and V_{in}= 571V.

The losses in the three-phase active PFC boost rectifier with the input voltage 571 V are shown in the form of pie chart in Figure 5.27.

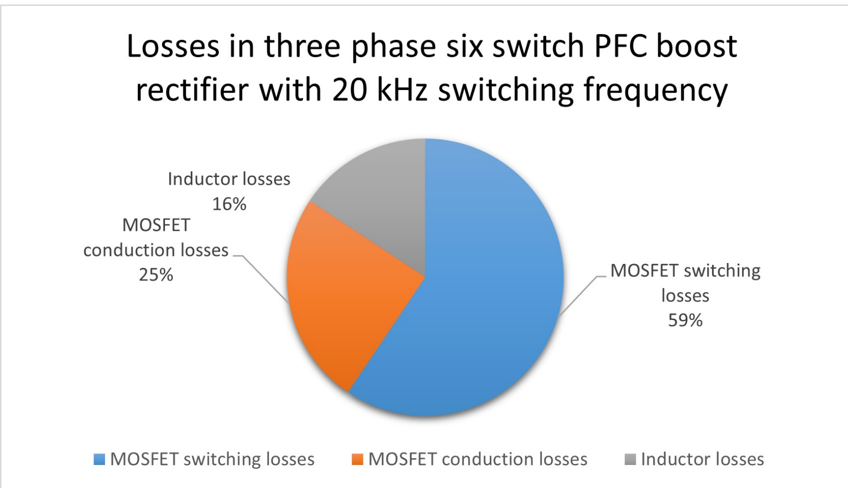

Figure 5.27: Losses in six switch PFC boost rectifier with 20 kHz and V_{in}= 571V.

With the results obtained from the LT Spice simulations, it is concluded that the best topology to integrate the grid with fast wireless charging system is the three-phase six switch active PFC boost rectifier.

6

Conclusion and Future Work

6.1 Conclusion

The electrification of ferries is sustainable since it directly addresses the urgent need to reduce CO_2 emissions, noise, and wave generation [40] from waterborne transportation. It saves energy compared to conventional, diesel-powered ferries. Electric ferries are also superior in terms of lower maintenance costs as diesel engine has more moving parts as compared to the electric motor in which only the bearings need maintenance.

They are some limitation on the electrification of ferries. These are mainly due to the battery capacity and its size. Also, in some harbor areas, the grids are not strong enough to charge the high-power batteries of electric vessels. Due to the restrictions on burning the worst quality marine fuel and strong air quality regulations, battery technology is getting more competitive and cost effective. But still, the electrification in the marine sector is not feasible for deep sea ships that sail more than 10 to 20 days in sea. It is more viable for ferries, supply ships, and tugboats.

Studies show that building an electric vessel is expensive than the conventional diesel- powered ship. Then there is a cost for the transformer and the other electrical infrastructure. Once it reaches the break-even point, then it is a saving.

IPT technology has the potential for implementation in small and medium-size passenger ferries and line ferries. Fast wireless charging of electric ferries using IPT technology, is a practical solution for charging the electric ferries with a tight schedule and short docking time.

In order to establish a connection between the fast wireless charging system and the grid, a three-phase PFC boost rectifier is used. Three-phase active six switch topology is the most promising topology in to get the constant DC voltage with fewer harmonics. The simulation results show that the efficiency and power factor have the most favorable figures for this topology.

6.2 Future work

Fast wireless charging of electric ferries can be applicable for large ferries. Studies can be carried out for different commuter vessels and cargo vessels to analyze their energy consumption, schedule, and docking time to implement the fast wireless charging using IPT technology.

The bidirectional feature of three-phase active six switch PFC boost rectifier topology can be studied and implemented. A prototype of a three-phase active switch six PFC boost rectifier can be build by using the simulation results and verified.

Bibliography

[1] Gustaver, M. (2020) A Chalmers University of Technology Master's thesis template for LaTeX. Unpublished.

[2] Octupus Energy. When Will Fossil Fuels Run Out?. Available from: https://octopus.energy/blog/when-will-fossil-fuels-run-out/.

[3] Sadia Anwar, Muhammad Yousuf Irfan Zia, Muhammad Rashid, Gerardo Zarazua de Rubens and Peter Enevoldsen. Towards Ferry Electrification in the Maritime Sector. Energies. 2020; 13(24):6506. Available from: https://doi.org/10.3390/en13246506.

[4] Siamak Karimi, Jon Are Suul and Mehdi Zadeh. Shore Charging for Plug-In Battery-Powered Ships: Power System Architecture, infrastructure, and Control. Article in IEEE Electrification Magazine September 2020. DOI: 10.1109/MELE.2020.3005699.

[5] Giuseppe Guidi, Jon Are Suul, Frode Jenset and Ingve Sørfonn. Wireless Charging for Ships, High-power Inductive Charging for Battery Electric and Plug-in Hybrid Vessels. DOI 10.1109/MELE.2017.2718829, Date of publication: 5 September 2017.

[6] Guidi, Giuseppe & Suul, Jon & Jenset, Frode & Sorfonn, Ingve. Wireless Charging for Ships: High-Power Inductive Charging for Battery Electric and Plug-In Hybrid Vessels. 2017. IEEE Electrification Magazine. 5. 22-32. 10.1109/MELE.2017.2718829.

[7] Chunwei Cai, Jinquan Liu, Shuai Wu, Yanyu Zhang, Longyun Jiang, Zhipeng Zhang and Jinpeng Yu. Development of a Cross-Type Magnetic Coupler for Unmanned Aerial Vehicle IPT Charging Systems; Citation information: DOI 10.1109/ACCESS.2020.2984361, IEEE Access.

[8] Electrical Academia. Available from: https://electricalacademia.com/batteries/battery-sizing-calculation-solved-example/.

[9] Tura på Gullmarsfjorden och upptäck Skaftö. Available from: http://dejligcruise.se/tura-pa-gullmarsfjorden/.

[10] Fathom World. *Sweden's latest and largest hybrid electric car ferry delivered*. Jul 2019. Available from: https://fathom.world/swedens-latest-and-largest-hybrid-electric-car-ferry-delivered/.

[11] FÄRJEREDERIET TRAFIKVERKET. TIDTABLE Vägfärja Gullmarsleden Finnsbo–Skår–Finnsbo.

[12] Vineetha Puttaraj, Yujing Liu. Review on Electric Ferries and Charging Technlogies. Project title :Elektrifiering av Marin Urbana Transportsystem – Förstudie Laddning. Project partners: AB Volvo Penta, Chalmers, ABB AB.

[13] Trafikverket website. Available from: https://www.trafikverket.se/en/startpage/about-us/Trafikverket/STA-Road-ferries/.

[14] Trafikverket website Available from: https://www.trafikverket.se/farjerederiet/farjeleder/Farjeleder-i-Stockholm213/Adelsoleden/.

[15] FÄRJEREDERIET TRAFIKVERKET.TIDTABLE Vägfärja Adelsöleden Adelsö–Munsö–Adelsö.

[16] V. Cirimele, F. Freschi and M. Mitolo. Inductive Power Transfer for Automotive Applications: State-of-the-Art and Future Trends. 2016 IEEE Industry Applications Society Annual Meeting, Portland, OR, USA, 2016, pp. 1-8, doi: 10.1109/IAS.2016.7731966.

[17] WÄRTSILÄ. Wireless Charging Available from:https://www.wartsila.com/insights/article/the-evolution-of-wireless-charging.

[18] Chunwei Cai, Jinquan Liu, Shuai Wu, Yanyu Zhang, Longyun Jiang and Zhipeng Zhang, Jinpeng Yu. Development of a Cross-Type Magnetic Coupler for Unmanned Aerial Vehicle IPT Charging Systems. In IEEE Access, vol. 8, pp. 67974-67989, 2020, DOI: 10.1109/ACCESS.2020.2984361.

[19] Mohd Fakhizan Romlie, Kevin Lau, Mohd Zaifulrizal Zainol, Mohd Faris Abdullah and Ramani Kannan.Performance of Inductive Coupled Power Transfer Versus the Coil Shape - Investigation Using Finite Element Analysis. MATEC Web of Conferences 225, 01017 (2018) UTP-UMP-VIT SES 2018.

[20] MIT. Inductance and Magnetic Energy. Available from:http://web.mit.edu/viz/EM/visualizations/notes/modules/guide11.pdf.

[21] Daniel Pehrman. Design Aspects of Inductive Power Transfer Systems for Electric Vehicle Charging.Licentiante Thesis at Chalmers University of Technology Technical Report No: R007/2019 ISSN:1403-266X.

[22] Y. Liu, P. A. Hu and U. K. Madawala. Maximum Power Transfer and Efficiency Analysis of Different Inductive Power Transfer Tuning Topologies. 2015 IEEE 10th Conference on Industrial Electronics and Applications (ICIEA), Auckland, New Zealand, 2015, pp. 649-654,doi: 10.1109/ICIEA.2015.7334190.

[23] S. Karimi, M. Zadeh and J. A. Suul. Shore Charging for Plug-In Battery-Powered Ships: Power System Architecture, infrastructure, and Control.In IEEE Electrification Magazine, vol. 8, no. 3, pp. 47-61, Sept. 2020, DOI: 10.1109/MELE.2020.3005699.

[24] Visit fredrikstad hvaler .Available from: `https://www.visitfredrikstadhvaler.com/en/product/?tlp=2141493&name=The-city-ferry-and-the-Old-Town-ferry`.

[25] Power Tech Sweden. Available from:`https://powertechsweden.com/byferga/`.

[26] Google map. Available from :`https://www.google.com/maps/@59.2074685,10.9492534,14z`.

[27] Fredrikstad kommune. Available from:`https://www.fredrikstad.kommune.no/tjenester/Vann-vei-trafikk/byfergene/`.

[28] Fredrikstad blad. Available from:`https://g.acdn.no/obscura/API/dynamic/r1/ece5/tr_700_5000_s_t/2019-07-07T12:06:53.000%2B0200/fred/2019/7/7/12/image1%2B%25281%2529.jpeg?chk=1E62DE`.

[29] WÄRTSILÄ. *MF Folgefonn*. Available from: `https://www.wartsila.com/marine/customer-segments/references/ferry/mf-folgefonn`.

[30] WÄRTSILÄ. *Wireless Charging*. Available from: `https://www.wartsila.com/marine/build/power-systems/shore-connections/wireless-charging`.

[31] Vineetha Puttaraj,Yujing Liu. Review on Electric Ferries and Charging Technologies.Project title: Elektrifiering Av Marin Urbana Transportsystem –Förstudie addning.Project number: 47924-1

[32] Transformer data sheet. NORATEL 3- phase transformers, High voltage 40-2000 kVA, IP23.

[33] Iskender Ires and Naci Genc.Power Electronic Converters in DC Micro-grid.DOI: 10.1007/978-3-030-23723-3_6.

[34] J. W. Kolar and T. Friedli. The Essence of Three-Phase PFC Rectifier Systems. 2011 IEEE 33rd International Telecommunications Energy Conference (INTELEC), Amsterdam, Netherlands, 2011, pp. 1-27, DOI:

10.1109/INTLEC.2011.6099838.

[35] Rohaizan Bin Saher. Three Boost Rectifier Design. Master thesis; Universiti Tun Hussein Onn Malaysia JULY 2012.

[36] Xinghui Wu. Analysis, Design and Implementation of High Performance Control Schemes for Three Phase PWM AC-DC Voltage Source Converter. Phd Thesis. National University of Singapore 2008.

[37] Mariusz Malinowski and Marin P. Kazmierkowski. Control in Power Electronics:Selected Problems; Chapter 11; Control of Three-Phase PWM Rectifiers. Elsevier Science & Technology, 2002.
Michael O'Loughlin. An Interleaving PFC Pre-Regulator for High-Power Converters. Texas Instruments.

[38] Data Sheet. CREEE C3M0016120K Silicon Carbide Power MOSFET, C3MTM MOSFET Technology, N-Channel Enhancement Mode.

[39] Data Sheet. CREEE CPM3-1200-0013A Silicon Carbide Power MOSFET, C3MTM MOSFET Technology, N-Channel Enhancement Mode.

[40] Thomas Bay Estrup. E Ferry Project: Report on societal, gender and ethical issues of exploitation. Available from: `https://ec.europa.eu/research/participants/documents/downloadPublic?documentIds=080166e5ac2189e4&appId=PPGMS`.

A

Appendix 1

A.1 Three Phase Transformer

The three phase transformer is modeled in LT Spice by using the specifications provided in the data sheet of the transformer. The Figure A.1 represent the LT Spice model of the transformer.

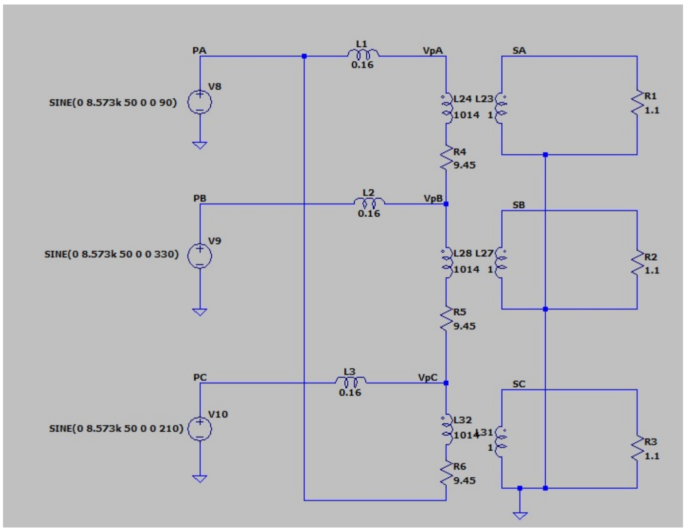

Figure A.1: Transformer model in LT Spice

The transformer has a vector group Dyn11 so

$$\frac{V_1}{V_2} = \frac{N_1}{\sqrt{3}N_2} \tag{A.1}$$

In LT Spice the transformer is modeled as coupled inductors. The value of inductor is calculated by using the number of turns.

$$\frac{L_1}{L_2} = \sqrt{\frac{N_1}{N_2}} \tag{A.2}$$

The values of the leakage inductance and resistance are calculated using the data sheet.

Table A.1: Transformer specifications [32]

Parameters	Values
Power kVA	315
Vector group	Dyn11
Primary line phase voltage	10.5 kV
Secondary line voltage	0.571 kV
Secondary phase voltage	0.329 kV
Primary line current	17.32 A
Primary phase current	10 A
Secondary line phase current	318 A
Total Cu losses W	3300 W
Cu losses per phase	1100 W
e_z	5.0 %
e_r	0.9%
Resistance per phase	9.45 Ω
Leakage reactance	0.16 H

The load for the transformer is PFC boost rectifier. It is modeled as resistive load. The power per phase of the transformer is 100 kW as the input power of the rectifier is assumed to be 300 kW.

$$R = \frac{V^2}{P} \tag{A.3}$$

$$R = 1.1\Omega \tag{A.4}$$

The primary and secondary voltages of the three phase are shown in Figure A.2. V(pi) represents the transformer primary voltage, V(si) represents the transformer secondary voltage and i is representing the phase of the transformer.

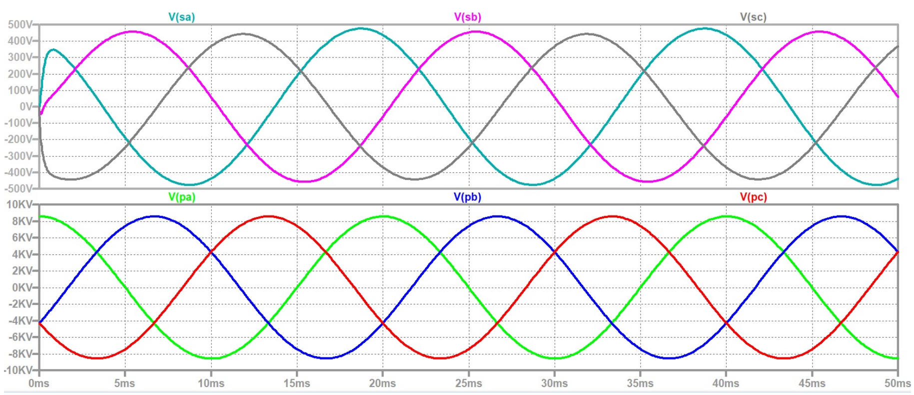

Figure A.2: Three phase transformer primary and secondary voltage.

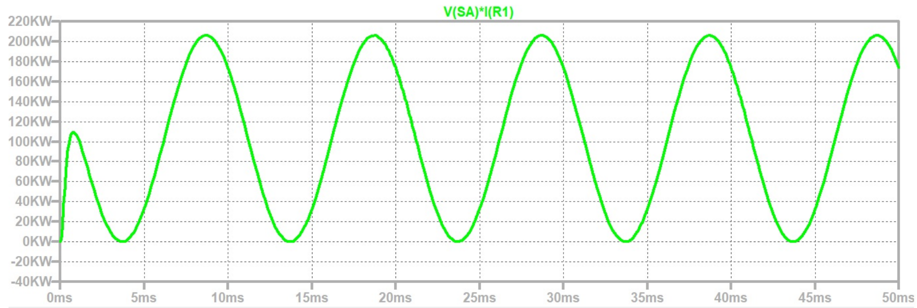

Figure A.3: Three phase transformer output power per phase.

The power dissipated across the per phase resistance of the the transformer is shown in Figure A.3. The average value of output power is 100 kW.

The copper losses are calculated using LT Spice which turns out to 900 W.

B

Appendix 2

B.1 Single Phase PFC Boost Rectifier

To evaluate the performance of the single phase PFC boost converter, same component as that of three phase circuit, are used to simulate the single phase PFC boost converter. The schematic of single phase PFC boost rectifier is shown in Figure B.1

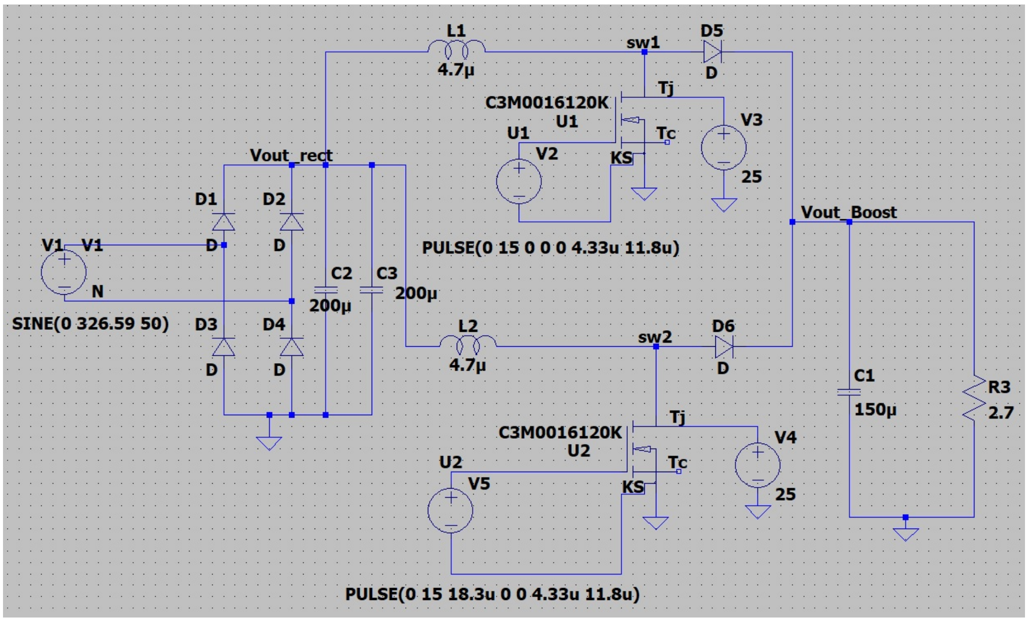

Figure B.1: Single phase interleaved PFC boost converter

The results of the single phase PFC boost converter are shown in Figure. B.2 and Figure. B.3.

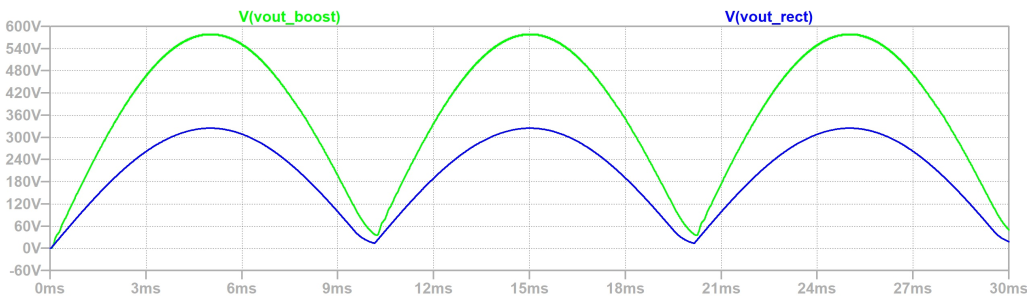

Figure B.2: Single phase simulation result: Output voltage.

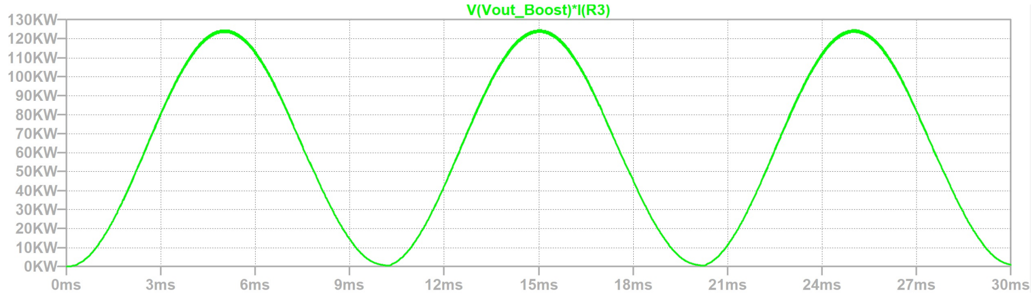

Figure B.3: Single phase simulation result: Output power.

The results are also presented Figure B.4

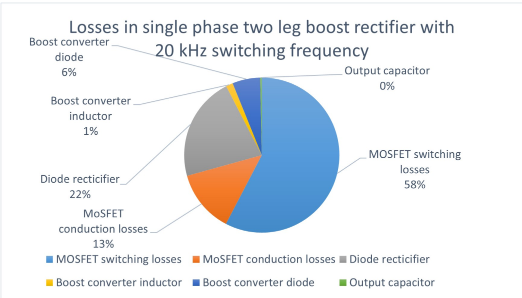

(a) Single phase 20 kHz.

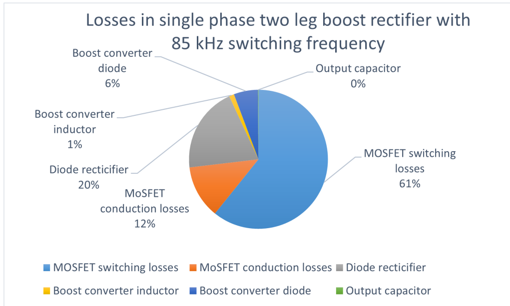

(b) Single phase 85 kHz.

Figure B.4: Losses in single phase PFC boost rectifier with 20 kHz and 85 kHz switching frequency.

DEPARTMENT OF SOME SUBJECT OR TECHNOLOGY
CHALMERS UNIVERSITY OF TECHNOLOGY
Gothenburg, Sweden
www.chalmers.se

AVANCEZ
1829
CHALMERS
UNIVERSITY OF TECHNOLOGY